computers

Tracked for Impact Factor

CITESCORE 3.7

Article

A Novel Criticality Analysis Technique for Detecting Dynamic Disturbances in Human Gait

Shadi Eltanani, Tjeerd V. olde Scheper and Helen Dawes

Special Issue

Advances of Machine and Deep Learning in the Health Domain

Edited by

Dr. Antonio Celesti, Dr. Ivanoe De Falco, Dr. Antonino Galletta and Dr. Giovanna Sannino

MDPI

https://doi.org/10.3390/computers11080120

computers

MDPI

Article

A Novel Criticality Analysis Technique for Detecting Dynamic Disturbances in Human Gait

Shadi Eltanani [1,*], Tjeerd V. olde Scheper [1] and Helen Dawes [2]

[1] School of Engineering, Computing and Mathematics, Faculty of Technology, Design and Environment, Oxford Brookes University, Wheatley Campus, Wheatley, Oxford OX33 1HX, UK; tvolde-scheper@brookes.ac.uk
[2] College of Medicine and Health, University of Exeter, St. Luke's Campus, Exeter EX1 2LU, UK; h.dawes@exeter.ac.uk
* Correspondence: seltanani@brookes.ac.uk

Abstract: The application of machine learning (ML) has made an unprecedented change in the field of medicine, showing a significant potential to automate tasks and to achieve objectives that are closer to human cognitive capabilities. Human gait, in particular, is a series of continuous metabolic interactions specific for humans. The need for an intelligent recognition of dynamic changes of gait enables physicians in clinical practice to early identify impaired gait and to reach proper decision making. Because of the underlying complexity of the biological system, it can be difficult to create an accurate detection and analysis of imbalanced gait. This paper proposes a novel Criticality Analysis (CA) methodology as a feasible method to extract the dynamic interactions involved in human gait. This allows a useful scale-free representation of multivariate dynamic data in a nonlinear representation space. To quantify the effectiveness of the CA methodology, a Support Vector Machine (SVM) algorithm is implemented in order to identify the nonlinear relationships and high-order interactions between multiple gait data variables. The gait features extracted from the CA method were used for training and testing the SVM algorithm. The simulation results of this paper show that the implemented SVM model with the support of the CA method increases the accuracy and enhances the efficiency of gait analysis to extremely high levels. Therefore, it can perform as a robust classification tool for detection of dynamic disturbances of biological data patterns and creates a tremendous opportunity for clinical diagnosis and rehabilitation.

Keywords: human gait; criticality analysis; support vector machine

Citation: Eltanani, S.; olde Scheper, T.V.; Dawes, H. A Novel Criticality Analysis Technique for Detecting Dynamic Disturbances in Human Gait. *Computers* **2022**, *11*, 120. https://doi.org/10.3390/computers11080120

Academic Editors: Antonio Celesti, Ivanoe De Falco, Antonino Galletta and Giovanna Sannino

Received: 30 June 2022
Accepted: 28 July 2022
Published: 3 August 2022

1. Introduction

The human gait is a central feature for humans [1], consisting of structured spatiotemporal interacting states that readily generate from variations in its dynamic initial state as a result of being externally or internally perturbed. When medical professionals want to obtain a rough estimate of the behaviour of human gait for better diagnosis, they just ask their patients to walk through for several steps and monitor the pattern of their walk. With this simple clinical examination, they can obtain valuable information from the way the person walks, which can help them detect the gait disturbances caused by casual deficiencies, such as dystonia, tremor, gait disorder, or other abnormal movement involved in the functional neurological system. These continuous disturbing interactions of gait have an impact on the global stability state of the biosystem. When the biosystem is exposed to such perturbation events, it exhibits an extreme sensitivity to its initial conditions and causes its behaviour to diverge exponentially from that of the unperturbed system and to operate in a chaotic behaviour that might be difficult to control. This opens the thinking horizons on how to control this chaos, which acts as external perturbations to the main biosystem, in order to maintain the global stability state to its overall function. How can these these external disturbances possibly be useful to detect abnormality in the motor system of human gait? This is what this paper aims at answering.

To begin with, it is imperative to understand the biological system function in terms of such a mathematical model, but unfortunately, some simplified or reduced models represented by a set of ordinary differential equations in the time domain prove to not sufficiently comprise the required complexity to characterise how the control mechanism that is responsible for translating the network behaviour into spatial outcomes in a biological system maintains global stable and controlled states. Regardless of the used representative biological model, the Rate Control of Chaos (RCC) [2] is considered as a robust bio-inspired metabolic feedback control mechanism that allows small perturbations to grow exponentially to perturb the biosystem, allowing it to stabilise any of the unstable periodic states that are involved inherently in it. The unstable periodic chaotic response, for example, can be suitably stabilised into a stabilised controlled periodic of oscillations by perturbing the operating conditions of the biosystem itself. Controlling the spatiotemporal changes or disturbances of gait patterns, on a smaller scale, requires tuning the biosystem parameters in both time and space. One of the best advantages of using the RCC concept is that it can be applied without prior knowledge of a specific mechanism of the biosystem but requires some instantaneous knowledge of some of the variables of the perturbed system, unlike the other control methods that require an accurate model to describe the biosystem in order to retain it into a stabilisation mode.

In this way, it is always possible, depending on the degree of applied disturbances, to guide chaotic gait disturbances into different nonlinear oscillatory controlled stable orbits. The interrelation between the biosystem perturbations and the amplitude of controlled chaotic orbits shows power-law and exponential relations. This also provides a structured representation at the edge of chaos of various biological properties such as those interconnected with the motor system of human gait, which can remotely reflect deep understanding of the underlying complex processes and their corresponding functionalities. This is what the proposed methodology of the Criticality Analysis (CA) does in this research paper. The CA technique allows nonlinear representation of the extracted human gait features that perturbed the biological function and accommodates them into a reduced lower-dimensional space. With the help of machine learning classification and categorisation models, it is possible to detect these disturbances of human gait. Due to the dynamics and nonlinearity of CA extracted features, a supervised machine learning algorithm based on the kernalised property of the Support Vector Machine (SVM) is implemented. The CA methodology interestingly proves its ability as a beneficial automation tool in the early diagnosis and detection of various pathological gait disorders and other unknown diseases associated with the biosystem.

The paper is organised as follows: Section 2 includes a description of human gait as a biological control system. In Section 3, the mathematical modelling of human gait is presented. Section 4 outlines the CA from machine learning perspectives and highlights the state-of-the-art work related to the SVM theory. In Section 5, the methodology of our MoRES dataset is discussed, including data collection, data analysis and feature extraction, criticality analysis as a data representation tool, the statistical analysis, the spatiotemporal analysis, the histogram analysis of CA data, and the SVM implementation mechanism that is followed by the confusion matrix as a performance measure. Section 6 discusses the experimental results of the MoRES dataset, focusing on the Receiver Operating Characteristic (ROC) Curve and the Area Under the Curve (AUC) as the most indicative performance measure metrics. Section 7 reflects on the experimental results obtained in Section 6. Lastly, Section 8 concludes the main findings of this research paper.

2. Human Gait as a Critical Control System

The motor system in humans, which is partially a subset of the global biosystem, is biologically complex, and no mathematical models are available to accurately describe its dynamics in both time and space domains. When such a disturbance occurs to a normal gait, the entire dynamic state of the biosystem chaotically drifts to a more critical state due to an excessive increase in the biosystem kinetic energy, and the behaviour may exhibit near

power-law and exponential relations. The interactions of the biosystem function within these disturbances create a very complex phenomenon, which thereby can be monitored just as the concentration of metabolic reactions in the biosystem was observed. The fluctuations in dynamics of the biosystem, which can hardly be interpreted as the nonlinear mechanism of local control of the motor system, can be controlled, but it also needs to be analytically modelled. The RCC method, which is proven recently as a robust technique to stabilise the nonlinear chaotic disturbance of a dynamic system, regulates the evolution rate of a nonlinear system such that the exponential growth of such an unstable chaotic oscillator is controlled into stable trajectories. The control is established using the rate of growth of some of the variables in proportion to the total embedded phase space of those variables. This is then used as an input variable to an exponential control function, which allows the rate of change of the variable to be controlled to accelerate or decelerate. When there is no control applied or the system is not exponentially changing, the proportional rate of change is unity.

Inspired by the traditional biochemical enzyme control concept that adjusts the reaction control [3], the RCC method is considered as a novel technique that can control the disturbances caused to the biosystem that could affect the other biological functions.

Controlling the reaction rate of biochemical reactions on the basis of the local information allows the biosystem to operate under a broad spectrum of certain conditions. This certainly can be extended further to control spatiotemporal chaos to achieve stability, such as the underlying dynamics of human gait. The stability of the overall biosystem trajectories must meet the Lyapunov stability, such that the biosystem can return to its equilibrium region of its phase space-controlled dynamics. The RCC has the ability to restore the perturbed biosystem to its normal stable state by applying localised control to some of its variables; however, it does not entirely suppress the underlying nonlinear behaviour of the biosystem, as it still contains some nonlinear properties, enabling it to respond to perturbations, and it can be less chaotic. Therefore, the RCC method does not eliminate entirely the chaotic properties of the underlying nonlinear system, but it applies limited localised control to the system to maintain an apparently stable system. The controlled system still has many properties of the nonlinear system, which can respond nonlinearly to weakly chaotic perturbations.

3. Mathematical Modelling of Human Gait

In this paper, the nonlinear biochemical enzyme control model by Berry [3] is being extended to describe the human gait function and the effect of its disturbance to the overall biosystem. Using the RCC method, the model, described by (4)–(7), has been proven to be controllable. The model applied a control to allow the stabilisation of the external perturbations to the motor system by calibrating the amount of enzyme taken into consideration for the concentration amount of one of the variables f. This model represents the control process of two enzymes that governs the formation of extracellular matrix m from soluble filaments f. The proteinase p alters the matrix into filaments, and the transglutaminase g brings back the filaments into matrix. The extracellular matrix m is generated by adjacent cells r_{im} at a constant rate, and each protein breaks down in catalytic processes proportional to p. The bifurcation parameter r_{im} acts as an external turbulent input to the control model, for which the biosystem loses its stability and resides in a chaotic state. The RCC is defined by the soluble filaments f given in (1) and the rate of change of the production of both enzymes p and g, which are described in (2) and (3). The output of this controlled model is described as a time series of the main varying parameters f and m or as a phase space plot, where f (x-axis) and m (y-axis).

$$\delta_f = \frac{f}{f + \eta_f} \tag{1}$$

$$\Theta_p(\delta_f) = f_p e^{(}\xi_p \delta_f) \tag{2}$$

$$\Theta_g(\delta_f) = f_g e^{(}\xi_g \delta_f) \tag{3}$$

$$\frac{dm}{dt} = k_g \frac{fg}{K_G + f} - \frac{mp}{1+m} + r_{im} \tag{4}$$

$$\frac{df}{dt} = -k_g \frac{fg}{K_G + f} + \frac{mp}{1+m} - \frac{fp}{1+f} \tag{5}$$

$$\frac{dp}{dt} = \Theta_p(\delta_f)\gamma \frac{f^n}{{K_R}^n + f^n} - k_a p^2 \tag{6}$$

$$\frac{dg}{dt} = \Theta_g(\delta_f)\beta \frac{f^l}{{K_S}^l + f^l} - k_{deg} \frac{gp}{K_{deg} + g} \tag{7}$$

The extended Berry model parameters are as follows: $\gamma = 0.026$, $\beta = 0.00075$, $K_R = 4.5$, $K_S = 1$, $K_G = 0.1$, $K_{deg} = 1.1$, $k_g = k_{deg} = 0.05$, $k_a = \frac{k_{deg}}{K_{deg}} = 0.0455$, and the Hill numbers $n = l = 4$. The r_{im} bifurcation parameter exhibits a wide spectrum of dynamic behaviours, including periodic stable limited cycles, bistability, and chaos. This parameter remains constant for all oscillators within the chaotic domain. In this extended model, an external input used as perturbations is applied to this r_{im} parameter as presented in (8). This parameter links different oscillators together by using a relative scale contribution from all other oscillators. In addition, the RCC control parameters shown in (1)–(3) ($f_p = f_g = 1$, $\xi_p = \xi_g = -1$, and $\eta_f = 2$) remain constant throughout the experiment simulations in this paper, although they can have different values that enable the local oscillator to change its oscillatory orbits.

$${r_{im}}^i = \sum_{j=1, j\neq i}^{n} w_j m_j + \varepsilon \tag{8}$$

where w_j represents the connectivity strength between various oscillators, which can be either 0.00011, 0.00012, or 0.00025. The ε is the uniform Gaussian distribution of the external perturbations applied to each oscillator, which is scaled over the domain $[-1, 1]$.

Moreover, the perturbation is observed graphically over a range of evolution steps used for the system to explore various perturbation values that result in different oscillatory cycles. In this paper, the connectivity strength value $w_j = 0.0002$ has been selected from the chaotic domain of the underlying oscillators. For each oscillator, this value may change to only affect the dynamics but not the overall stability.

The implemented RCC controlled method of the extended Berry model has been shown to stabilise the local nonlinear spatiotemporal patterns of the human gait. The RCC method performs effectively when the response of the underlying system is chaotic. This method enhances the stability of nonlinear systems into stabilised periodic limited cycles according to the local dynamic behaviour of each dynamic oscillator.

In this paper, the network of nonlinear models consists of 16 oscillators, such that each individual oscillator can adjust its local dynamics to accommodate the external perturbations by their adjacent neighbours. The total model is simulated by EuNeurone software [4] using Fehlberg-RK as an Ordinary Differential Equation (ODE) fixed step integration method. The total unweighted dynamics M and F as in (9) and (10) is measured by the net sum of the individual oscillators that could be seen by a remote observer whose individual oscillators are invisible.

$$M = \sum_{i=1}^{n} m_i \tag{9}$$

$$F = \sum_{i=1}^{n} f_i \tag{10}$$

The biochemical enzymes control of the Berry model is recognisably applicable for several types of control needed for biological control processes, such as the motor system of the human gait. The RCC method has mainly been used to control many different models, including Rossler, Lorenz, and Grey–Scott models [5,6] to analytically model biological patterns of the release process of insulin in critical systems.

4. Related Work

4.1. Criticality Analysis: from Machine Learning Perspectives

The main objective of the research work in this paper is to provide a novel data representation methodology for human gait that has the ability to accommodate high-dimensional nonlinear data points in a reduced features space; thereby, the machine learning automation techniques can be applied for detection and categorisation purposes. It has been shown that the RCC-controlled Berry model stabilises the external disturbances that perturb its system into periodic stable trajectories.

In a technical way, the total response of the RCC-controlled Berry model represents the extracted dynamics involved in human gait patterns in terms of the extracellular matrix variable m from the soluble filaments variable f, and this is the basis of the novel Criticality Analysis (CA) methodology. The CA is a feasible method that allows a useful scale-free representation of multivariate dynamic data in a nonlinear representation space. In this method, each data sample is characterised by a unique orbit, resulting from the original data samples perturbing the underlying critical system. Such a critical system is composed of a network of nonlinear controlled oscillators. The scale-free network of orbits is a quantitative measure of a non-scale-free interacting set of patterns or attributes that arise from the whole complex biological function, and it reveals organised features of the structure of dynamic properties interconnected with human gait.

To the best of our knowledge, there is no research work that considers the CA technique, based on the RCC method, as a biological feature extraction technique. This research paper is the first to formulate an RCC-controlled biological mathematical model for human gait based on the Berry model that analyses the dynamic interactions and detects gait disturbances, affecting the normal walking in humans.

Based on the developed CA technique, this paper focuses on providing a unique reliable solution using one of the robust supervised machine learning algorithms, e.g., Support Vector Machines (SVM) in identifying nonlinear relationships and high-order interactions between multiple gait data variables that may be challenging for traditional statistics.

The Algorithm 1 proposed in this paper uses the advanced kernelised feature of the SVM that increases the accuracy and enhances the efficiency of gait analysis to extremely high levels. My original algorithm was applied on the Movement, Occupational and Rehabilitation Sciences (MoRES) Dataset: a collected real-time experiment by the Faculty of Health and Life Sciences at Oxford Brookes University.

4.2. Support Vector Machine (SVM)

4.2.1. Overview of SVM

SVM is a powerful machine learning technique that is used mainly for learning from data, in particular, for performing binary classification and regression estimation tasks [7–9], such as disease diagnosis, image classification, face recognition, etc. Due to the nonlinear structure of data and the complexity of classification problems, the SVM is developed to form a nonlinear class decision boundary by means of a kernel technique. The SVM aims at establishing an optimal separating hyperplane (OSH) and thereby maximises the margin between various classes. Through the kernel technique, the fundamental bases of SVM input data are to transform input data into a high-dimensional space and then to create an OSH to classify various data labels in the transformed feature space. The linear OSH leads to the formulation of a nonlinear boundary in the original data input space. The data vectors closest to the OSH in the transformed space are called the support vectors, which contain

deep knowledge about the OSH. In most real-time applications, the selection of the kernel is crucial, as it has an impact on the classification's accuracy.

4.2.2. Basic Theory of SVM

Given that a training dataset $\Omega = \{(\boldsymbol{x_i}, y_i)\}_{i=1}^{N}$ is drawn independently from a probability distribution on $(\mathcal{X}, \mathcal{Y})$, with $\mathcal{X} \in \mathbb{R}^m$ as the input features and $\mathcal{Y} \in \{-1, +1\}$ as a classification output. The SVM model achieves for linearly separable patterns in m dimensional space an optimal separating kernel generated decision function $\boldsymbol{w^T}\phi(\boldsymbol{x_i}) + b = 0$ by minimising an adequate trade-off between the structural empirical risk and the model complexity of its optimisation problems. The $w_\circ$ is the optimal adjustable weight vector and $b_\circ$ is the optimal bias of the decision function, where both of those values are defined when the feature vectors $\boldsymbol{x_i}$ maximised. For any two arbitrary classes $\{-1, +1\}$, the SVM finds two parallel hyperplanes that correctly classify all training data points and maximise the distance $\frac{2}{\|w\|}$ or minimise the margin $\frac{1}{2}\|\boldsymbol{w}\|^2$ between them. For each linearly separable case, the SVM standard classification optimisation problem can be expressed mathematically as:

$$\begin{aligned} \min_{\boldsymbol{w},b} \quad & \frac{1}{2}\|\boldsymbol{w}\|^2 \\ \text{subject to} \quad & y_i(\boldsymbol{w^T}\phi(\boldsymbol{x_i}) + b) \geq 1 \end{aligned} \tag{11}$$

The resulting SVM classifier $y_i = \text{sign}(\boldsymbol{w^T}\phi(\boldsymbol{x_i}) + b)$ determines each class on either side of the hyperplane. Both $\min(\boldsymbol{w^T}\phi(\boldsymbol{x_i}) + b) = 1$ and the $\max(\boldsymbol{w^T}\phi(\boldsymbol{x_i}) + b) = -1$ hold when $y_i = +1$ and $y_i = -1$ satisfy the conditions, respectively. In most real-life practical scenarios, the data points can either be within the margin space or even on the wrong side of the decision boundary, which makes the classification problem more challenging and complex. In this case, a soft margin approach based on the slack variables ξ_i is introduced to solve this problem of non-separable data in a simple and effective manner. The primal form of the SVM in (11) can be re-written as:

$$\begin{aligned} \min_{\boldsymbol{w},b,\xi} \quad & \frac{1}{2}\|\boldsymbol{w}\|^2 + C\sum_{i=1}^{n}\xi_i \\ \text{subject to} \quad & y_i(\boldsymbol{w^T}\phi(\boldsymbol{x_i}) + b) \geq 1 - \xi_i \\ & \xi_i \geq 0 \end{aligned} \tag{12}$$

where C is the user-supplied regularisation parameter, which controls the trade-off between the maximum margin and loss. In (12), either $y_i(\boldsymbol{w^T}\phi(\boldsymbol{x_i}) + b) \geq 1$ and $\xi_i = 0$ as before in (11), or $y_i(\boldsymbol{w^T}\phi(\boldsymbol{x_i}) + b) < 1$, and then $\xi_i > 0$ takes the value satisfying $y_i(\boldsymbol{w^T}\phi(\boldsymbol{x_i}) + b) = 1 - \xi_i$.

The SVM uses the Hinge loss function to measure the empirical risk of the given training data points satisfying $y_i(\boldsymbol{w^T}\phi(\boldsymbol{x_i}) + b) < 1$. These data points that lie near the boundary of the separating hyperplane can be noisy, which can mislead the resulting separating hyperplane. For minimizing the model complexity, the SVM minimises a regularization term in their optimization problem. Ideally, the standard form of (12) becomes:

$$\min_{\boldsymbol{w},b} \quad \frac{1}{2}\|\boldsymbol{w}\|^2 + C\sum_{i=1}^{n}\theta\Big(y_i(\boldsymbol{w^T}\phi(\boldsymbol{x_i}) + b)\Big) \tag{13}$$

with the Hinge loss function θ:

$$\theta(\alpha) = (1 - \alpha) = \begin{cases} 1 - \alpha, & 1 - \alpha > 0 \\ 0 & \text{otherwise} \end{cases}$$

The optimisation problem of (12) incorporated with (13) can be mapped to a constrained optimisation problem with linear constraints and global minimum. The details of evaluating the optimal values of $w_\circ$ and $b_\circ$ can be found in [7,10]. For simplicity, the bias or the offset parameter b can be ignored, and the output of the prediction function f

can be parameterised by $\boldsymbol{w}$ as $f(x) = \langle \boldsymbol{w}, \phi(\boldsymbol{x_i}) \rangle$. Therefore, the SVM model in (13) aims at solving the optimisation problem:

$$\min_{w \in \mathbb{H}} \quad \frac{1}{2}\|\boldsymbol{w}\|^2 + C\sum_{i=1}^{n} \theta(y_i, \langle \boldsymbol{w^T}, \phi(\boldsymbol{x_i}) \rangle) \tag{14}$$

where $\mathbb{H}$ is a Reproducing Kernel Hilbert space (RKHS) induced by a kernel function $\kappa(\phi(\boldsymbol{x}), \phi(\boldsymbol{z}))$ with a feature mapping function $\phi : \mathbb{R}^m \mapsto \mathbb{H}$. For nonlinear problems, the SVM model of (14) cannot be solved efficiently due to the fact that $\phi(\cdot)$ is always a high-dimensional and even infinite mapping function. By using the representer theorem [11], there exists a vector $\beta^* \in \mathbb{R}^m$ such that the solution of (14) holds $\boldsymbol{w}^* = \sum_{i=1}^{m} \beta_i^* \phi(\boldsymbol{x_i})$. By substituting $\boldsymbol{w} = \sum_{i=1}^{m} \beta_i \phi(\boldsymbol{x_i})$ in (14), the equivalent finite dimensional optimisation problem can be presented as follows:

$$\min_{\beta \in \mathbb{R}^m} \quad \frac{1}{2}\|\boldsymbol{w}\|^2 + C\sum_{i=1}^{n} \theta(y_i, \boldsymbol{K}_i \beta_i) \tag{15}$$

where $\boldsymbol{K}$ is the kernel matrix that satisfies $\boldsymbol{K}_{i,j} = \kappa(\boldsymbol{x}_i, \boldsymbol{x}_j)$ and $\boldsymbol{K}_i$ is the $k-$th row of $\boldsymbol{K}$. The coefficient β_i is bounded [10], as $0 \leqslant \beta_i \leqslant C$.

The Gaussian kernel function is commonly used in the capacity control and regularisation of radial basis function (RBF) networks [12], which takes the form $\boldsymbol{K}_{i,j} = \kappa(\boldsymbol{x}_i, \boldsymbol{x}_j) = \exp\left(\frac{-\|\boldsymbol{x}_i - \boldsymbol{x}_j\|^2}{2\sigma^2}\right)$, whose function space is based on the norm in RKHS. When the data points $\boldsymbol{x}_i$ move away from the centre $\boldsymbol{x}_j$, the function monotonically decreases. The width parameter σ controls the rate at which the RBF function decreases and is inversely proportional to its norm [13].

5. Methodology

This section outlines the proposed methodology framework, consisting of data collection, data processing, features extraction technique and the implementation of the SVM classifier. The flowchart of the methodology is shown in Figure 1.

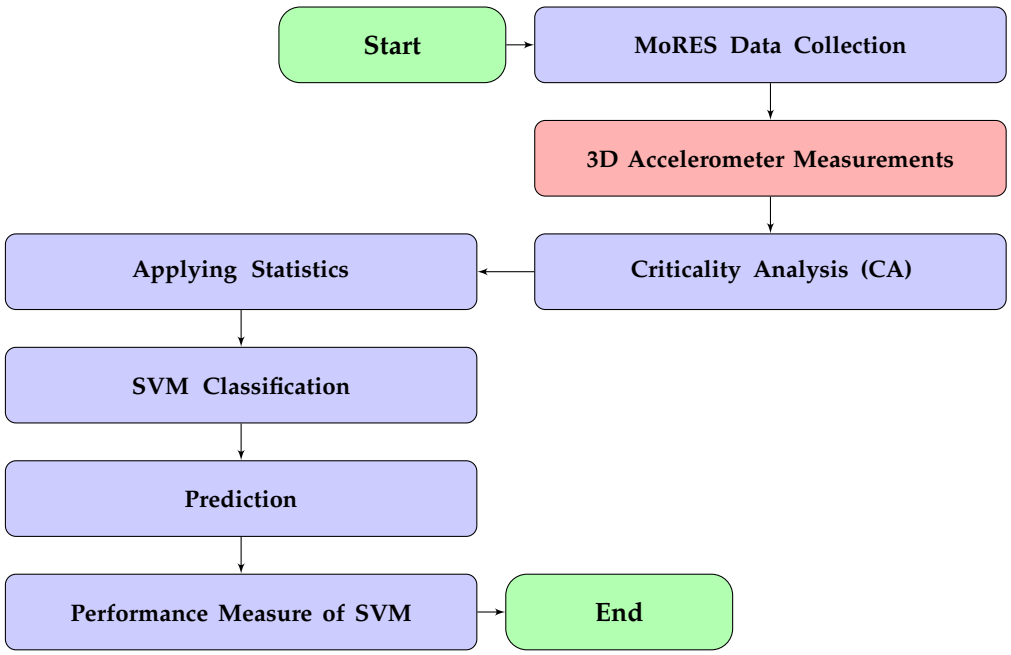

Figure 1. The flowchart of the proposed methodology.

5.1. Data Collection

Participants who are at the adult age and with healthy normal walk together with disturbed walk known as strapped walk and attended the Movement, Occupational and Rehabilitation Sciences (MoRES) centre at the Faculty of Health and Life Sciences at Oxford Brookes University in the UK were offered participation in a provisional clinical study to support the Criticality Analysis of Gait in Adults (CAGA) project. All participants provided informed consent prior to participation. The critical pathology characteristics of participants were psychologically measured by a medical professional prior to and during the walking exercise in order to (1) measure their ability to walk independently as a primary means of mobility and (2) determine the underlying causes of their health conditions as well as their level of motivation to follow the program during the clinical study. A healthy group of individuals, who are free from peripheral injury or other conditions preventing their mobility without assistive devices, was also recruited to participate in the trial.

For a feasible outcome of the clinical experiment, the participants consisting of five individuals were asked to walk back and forth on a flat surface over a period of 6 s. Critical changes in walking control, stride frequency, and length of steps were observed as individuals change speed, effectively stressing their mobility.

The assessment is based on the use of a movement sensor, which is placed on the fourth lumbar vertebra that is located on the top left of the anatomical position of lumbar spine, acting as the body Centre of Mass (CoM). It is designed to be incredibly flexible, providing for mobility in many different planes including flexion, extension, side bending, and rotation. The single built-in Inertial Measurement Unit (IMU) sensor helps determine the motion, orientation and heading of the body motor function [14]. The participants were provided with with a wrist-worn Axivity AX3 triaxial accelerometer, which measures linear acceleration from $^{+}/_{-}$ 2 g to $^{+}/_{-}$ 16 g range along three orthogonal axes known as z (upward and downward), y (left and right) and x (forward and backward), to record and track their physical activity. The dynamics of their walking activity during the assessment is monitored using the Polar Team tracking system [15].

The operating procedures of the data collection are as follows:

(1) The IMU movement sensor unit is used to collect the gait data for each participant, and the wrist-worn Axivity AX3 accelerometer, which is worn on the non-dominant wrist, is utilised to record the participant's physical activity.
(2) The AX3 accelerometer is connected to a laptop USB hub using a Micro USB cable for data transfer, and then, the collected data are internally stored on a one Terabyte (1TB) memory size as a raw binary file.
(3) The collected data can be read by using the AX3 OMGUI software, which is installed on a laptop. Details on how to install the software together with the configuration setup of data recording are documented in [16].
(4) The Movement, Occupational and Rehabilitation Sciences centre at the Faculty of Health and Life Sciences at Oxford Brookes University supervised the entire process of data collection and the collected data had been named as the MoRES dataset in recognition of their contribution as a data provider centre.
(5) Under the rules of General Data Protection Regulation (GDPR), the collected MoRES dataset has been anonymised and shared via a secured Google drive folder with the School of Engineering, Computing and Mathematics (ECM) at Oxford Brookes University for research purposes, where it underwent official approval procedures by the University Research Ethics Committee (UREC).
(6) The MoRES dataset contains the raw collected data from the 3D IMU sensory unit. For each participant, there are two groups of measurements: normal walk patterns (well-apparent gait subjects) and strapped walk patterns (ill-apparent gait subjects). Each group of data is used as an input to the CA methodology described by (4)–(7) for multivariate data representation, such that the measurements of the 3D IMU features can be reduced to only two represented features. Details on this are discussed in Section 5.2.

5.2. Data Analysis and Feature Extraction

The MoRES dataset, which is collected by using a single three-dimensional accelerometer, gyroscope and magnetometer IMU sensor, was analysed using the RCC Berry model described by (4)–(7), which is developed in EuNeurone software [4]. The criticality analysis dominant features f (x-axis) and m (y-axis), associated with each walk pattern for each individual gait, were extracted and used for the classification task in this paper. The advantage of using those spatiotemporal parameters f and m is to describe the development of human gait dynamic patterns, represented by the phase space portrait analysis, which allows the discovery of variability of different gait patterns structure.

5.3. Criticality Analysis as a Data Representation Method

The Criticality Analysis method shows that a controlled self-organised critical system can be constructed from RCC-controlled networks of oscillators. These can then be used to uniquely represent arbitrary data in a nonlinear representation space that allows readily classification without training. Each data sample is characterised by a unique orbit. This orbit is the result of the data samples perturbing the underlying critical system. The system is critical due to the fact that it is made by a network of nonlinear controlled oscillators. The critical property is emergent from this network, such that any small change in any of the input causes a change of state in the orbit of the total network, yet it will not become unstable. The resulting orbit is therefore a scale-free representation of the original data and can then be used to show that a specific set of attributes that represents the gait of an individual patient or control is similar to the matching category of the sample versus the other data members [17]. The representation helps reduce the dimensionality of the dynamic data.

Figures 2–6, the phase space plots of the CA data representation for each categorised group of participants, are shown, respectively. The phase plot shown in Figure 7 represents each walk category for all individuals, where the normal walk behaviour is characterised by more variability in the phase space in comparison to that of strapped walk patterns. This means that the individual's healthy normal gait is free from disturbances and there has been no effort made to complete the cycle of walk. The strapped gait of individuals shown in Figure 7 has extreme overlapped walk patterns, which makes it complex to understand and to extract useful information. Figures 2–7 illustrate that the healthy and affected gait patterns can be detectable and classifiable in a time domain, even without machine learning training. The dynamic representation of individual data samples can then be used to compare between categories and even to monitor the progression of data over time. These properties of CA are used in this paper to show how normal walk patterns differ from their counterparts of strapped walk patterns. This normal gait is shown to have a large variability and more structured patterns that underpin the ability of individuals with normal gait to move without physical restrictions as is characterised by their changing behaviour among the participants. Strapped walk behaviour is more restricted in their ability to vary their gait, which is not normally recognisable from the data, as this is highly nonlinear.

It is noticeably shown in the normal phase plots, visualised on the left side of Figures 2–7, that the external perturbations to the network of coupled oscillators can boost or reduce the gait behaviour patterns due to the scaled additive connectivity strength to the external perturbations, ensuring that the perturbed input to each oscillator is not heavily great to obtain the response of the system out of the controlled domain.

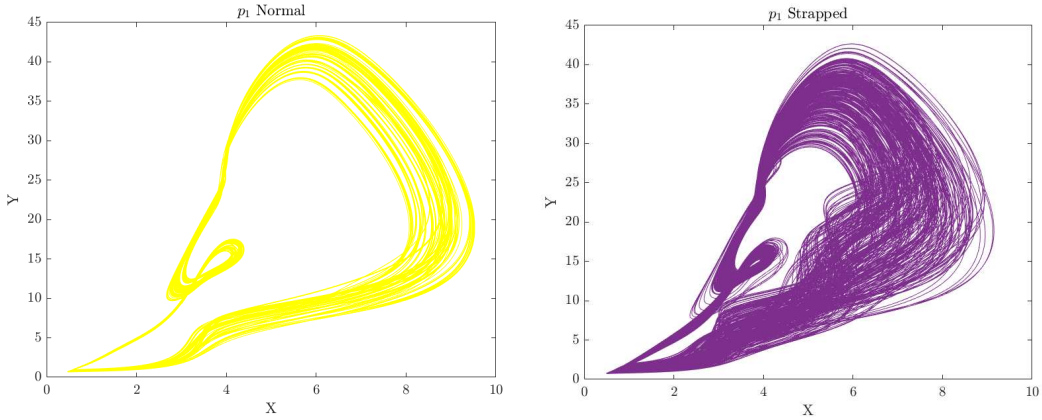

Figure 2. This figure shows the phase space plots for each walk pattern that correspond to individual of p_1. On the left is the normal walk patterns portrait, while the strapped patterns are on the right side of Figure 2.

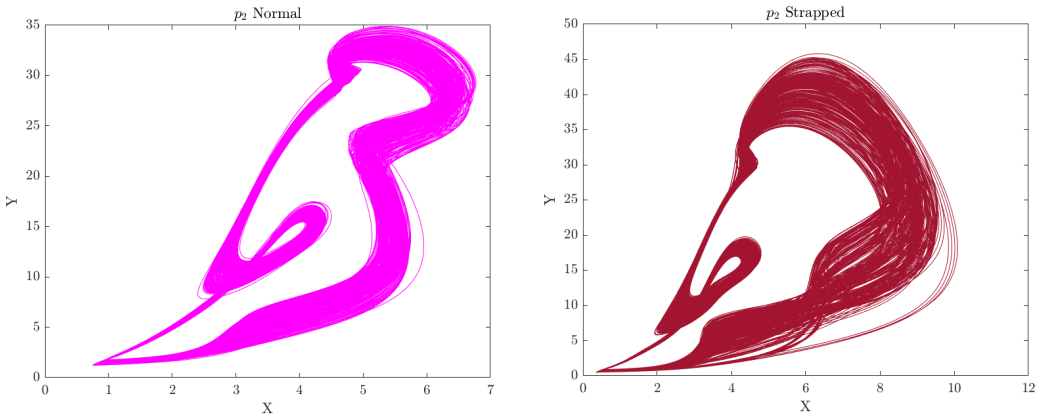

Figure 3. This figure shows the phase space plots for each walk pattern that correspond to individual of p_2. On the left is the normal walk patterns portrait, while the strapped patterns are on the right side of Figure 3.

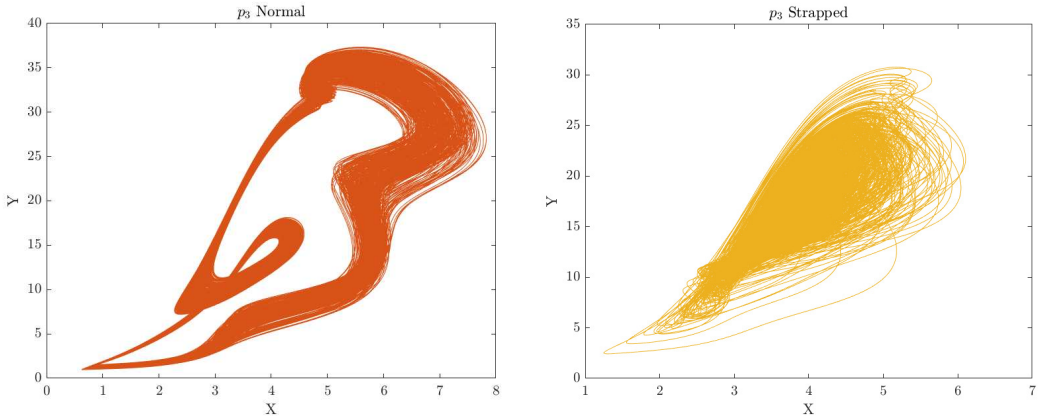

Figure 4. This figure shows the phase space plots for each walk pattern that correspond to individual of p_3. On the left is the normal walk patterns portrait, while the strapped patterns are on the right side of Figure 4.

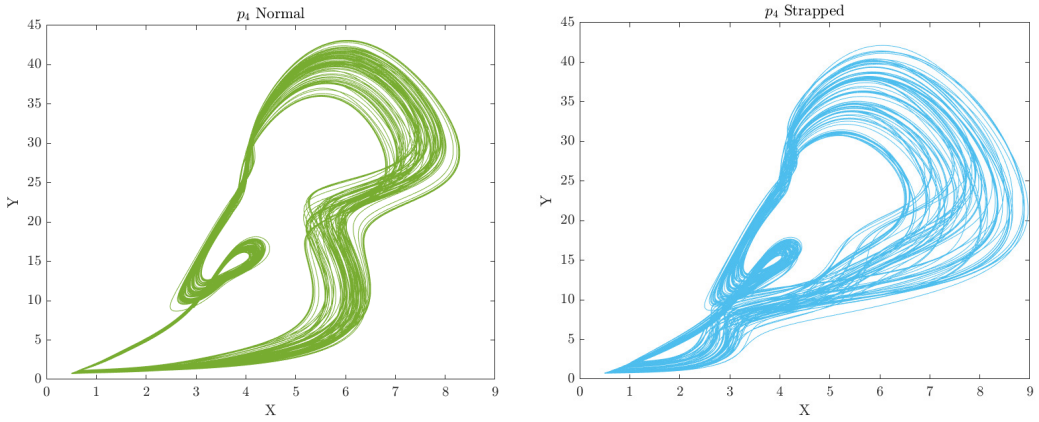

Figure 5. This figure shows the phase space plots for each walk pattern that correspond to individual of p_4. On the left is the normal walk patterns portrait, while the strapped patterns are on the right side of Figure 5.

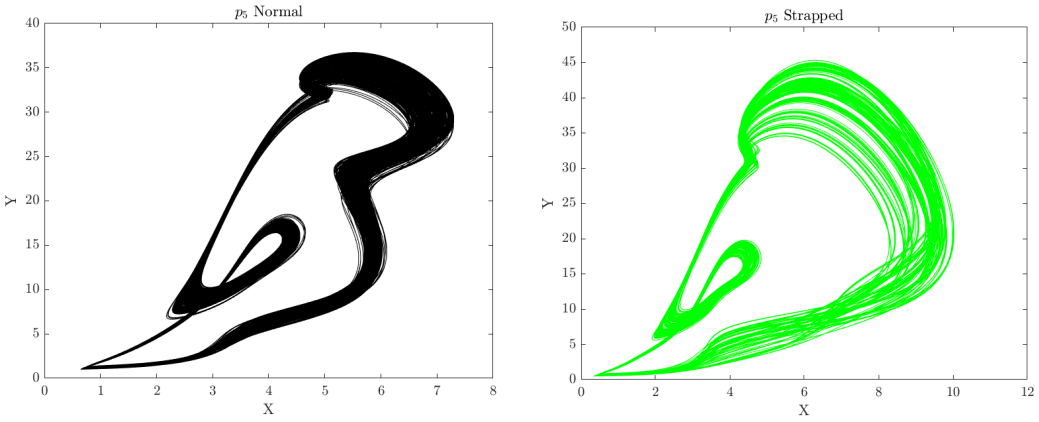

Figure 6. This figure shows the phase space plots for each walk pattern that correspond to individual of p_5. On the left is the normal walk patterns portrait, while the strapped patterns are on the right side of Figure 6.

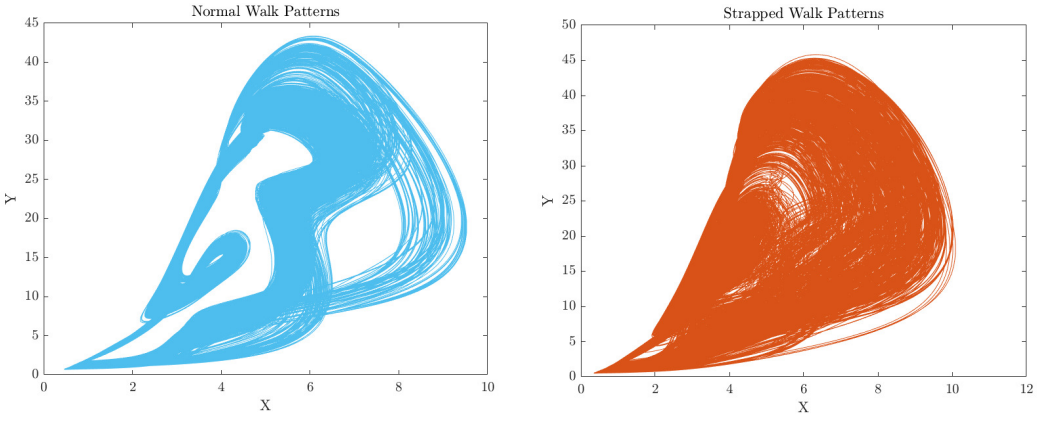

Figure 7. This figure shows the phase space plots for each walk pattern for all individuals of the same category. On the left is the normal walk patterns portrait, while the strapped patterns are on the right side of Figure 7.

5.4. Statistical Analysis of CA Data

5.4.1. Scatter Analysis

The distribution of CA data representation for each individual walk pattern is shown in Figures 8–13, which interprets the figures depicted in Figures 2–7. Each plot describes the variability of continuous or successive gait interaction events over time the individual

takes. Since CA data show a degree of association between the two dominant extracted features in the 2D space, the Pearson's correlation coefficient ρ, bounded by $0 \leq \rho \leq 1$, quantitatively measures both the direction and strength of the dependency of extracted features on each other. The average of ρ for the normal walk patterns of all individuals is shown to be highly stronger and positive than the strapped patterns. In other words, the effect of ρ of the strapped features decreases steadily by 0.28% on average more than that of the normal patterns.

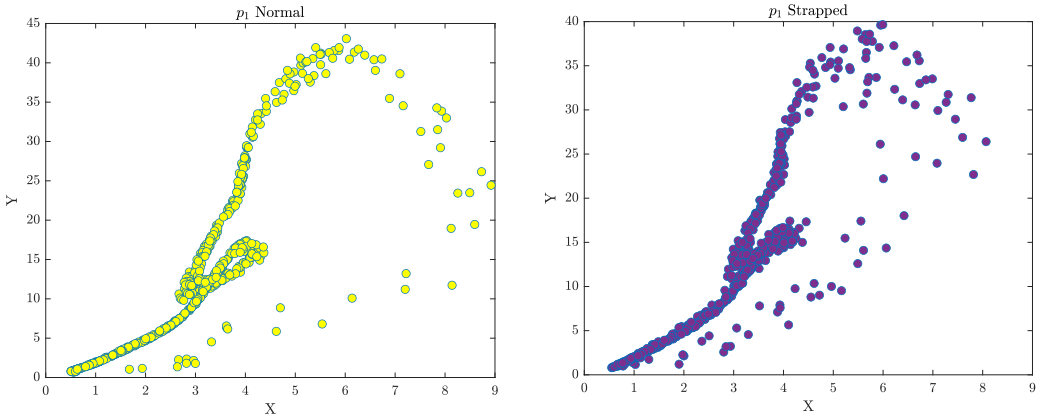

Figure 8. This figure shows the scatter plots for each walk pattern that correspond to the individual p_1. On the left is the normal walk patterns distribution, while the strapped patterns distribution is on the right side of Figure 8.

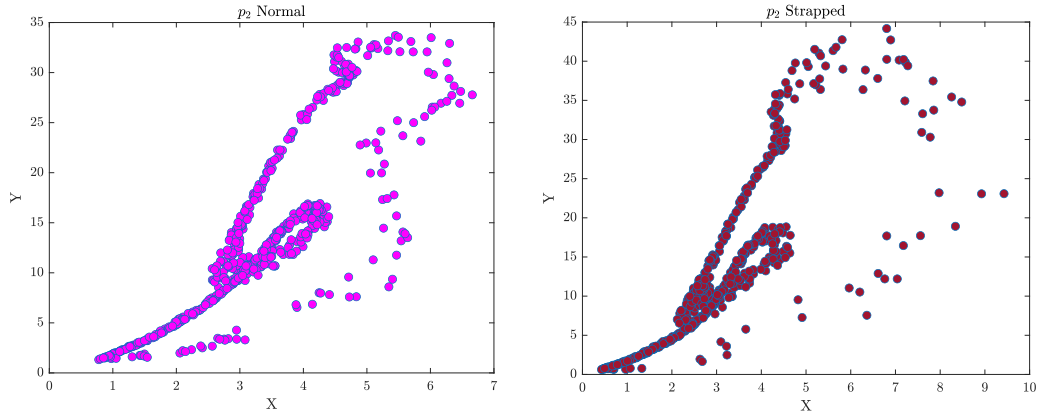

Figure 9. This figure shows the scatter plots for each walk pattern that correspond to the individual p_2. On the left is the normal walk patterns distribution, while the strapped patterns distribution is on the right side of Figure 9.

The right hand side of Figures 8–13, which corresponds to the strapped gait, show that there is an observable intensity of data points over the data space range or even irregularities in the spread of data samples, which make them different to the normal walk, as in the case in Figure 10.

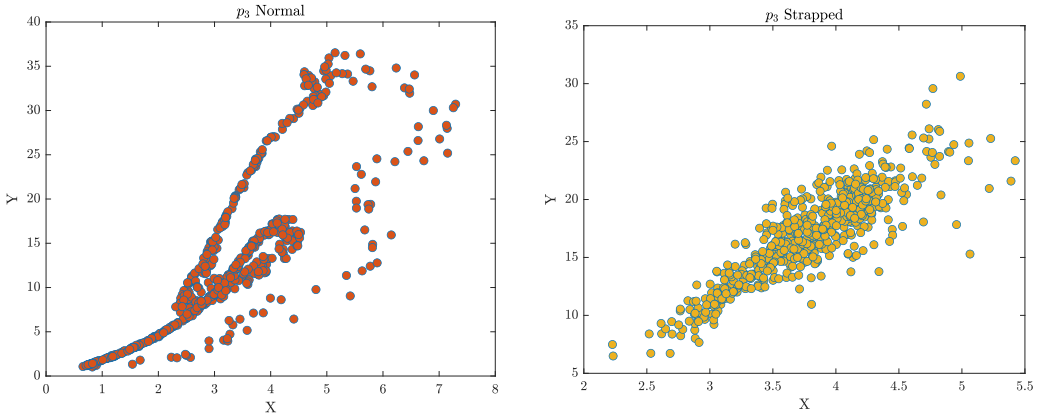

Figure 10. This figure shows the scatter plots for each walk pattern that correspond to the individual p_3. On the left is the normal walk patterns distribution, while the strapped patterns distribution is on the right side of Figure 10.

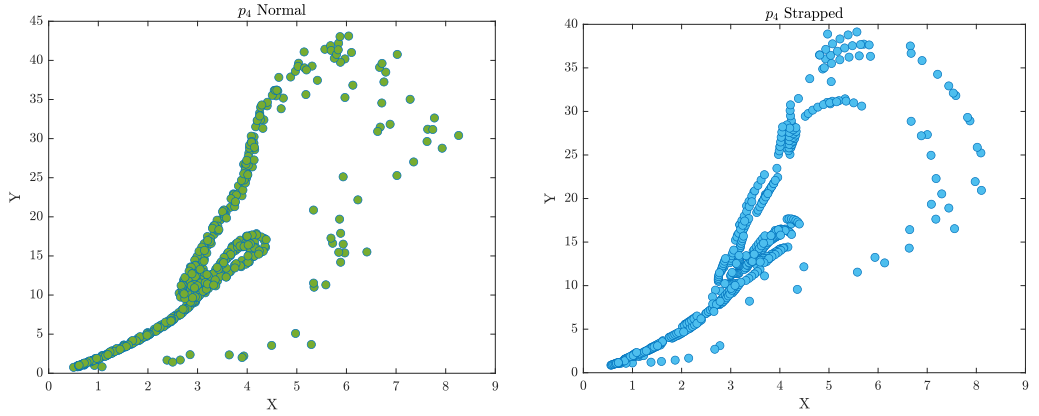

Figure 11. This figure shows the scatter plots for each walk pattern that correspond to the individual p_4. On the left is the normal walk patterns distribution, while the strapped patterns distribution is on the right side of Figure 11.

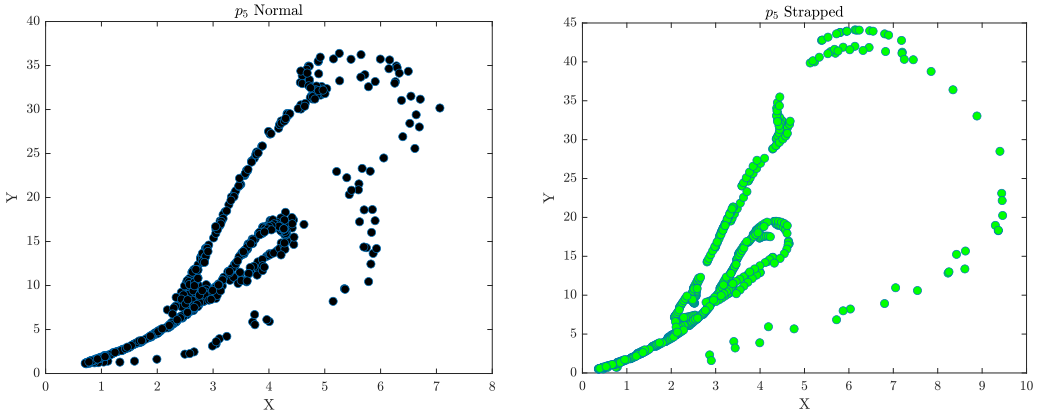

Figure 12. This figure shows the scatter plots for each walk pattern that correspond to the individual p_5. On the left is the normal walk patterns distribution, while the strapped patterns distribution is on the right side of Figure 12.

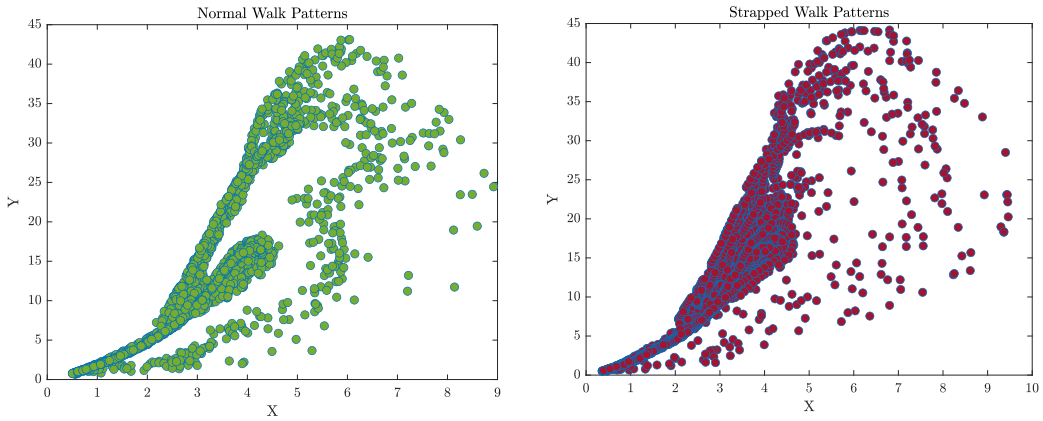

Figure 13. This figure shows the scatter plots for each walk pattern for all individuals of the same category. On the left is the normal walk patterns distribution, while the strapped patterns distribution is on the right side of Figure 13.

The values of ρ of different walk patterns for each individual and for all individuals from the same category are summarised in Tables 1 and 2, respectively, as follows:

Table 1. The correlation coefficient ρ of p_1, p_2, p_3, p_4 and p_5.

Category	Correlation Coefficient (ρ)				
	p_1	p_2	p_3	p_4	p_5
Normal Walk	0.815	0.846	0.832	0.84	0.847
Strapped Walk	0.86	0.819	0.871	0.838	0.778

Table 2. The correlation coefficient ρ of all individuals.

Category	Correlation Coefficient (ρ)
	All Individuals
Normal Walk Patterns	0.8337
Strapped Walk Patterns	0.8255

Each gait category whether it is normal or strapped has two dominant features, which are extracted from the RCC Berry model presented in Equations (4)–(7), where f of Equation (5) represents (x-axis) and m of Equation (4) is on the y-axis.

5.4.2. Spatiotemporal Analysis

Figure 14, which compares the normal gait dynamic patterns to strapped patterns, graphically shows that the gait dynamic disturbances have a significant effect on the progression of gait. It particularly illustrates and detects the location and variations of gait patterns between individuals suffering from certain gait abnormalities. The middle line of each categorical box represents the median. The amount of difference in the variability of data between each category for each individual measures the degree of dispersion and skewness of the CA data. Table 3 describes the median values of CA data for each category. The measurements indicated that the median of the CA data of the strapped walk patterns is decreased by 55.58% compared with that of the normal walk patterns. Furthermore, there are parallel lines, known as whiskers, which depict the variability of data outside the limits of the quartiles interval. It also appeared that most CA data are free of the outliers except that of the strapped patterns of the individual p_3.

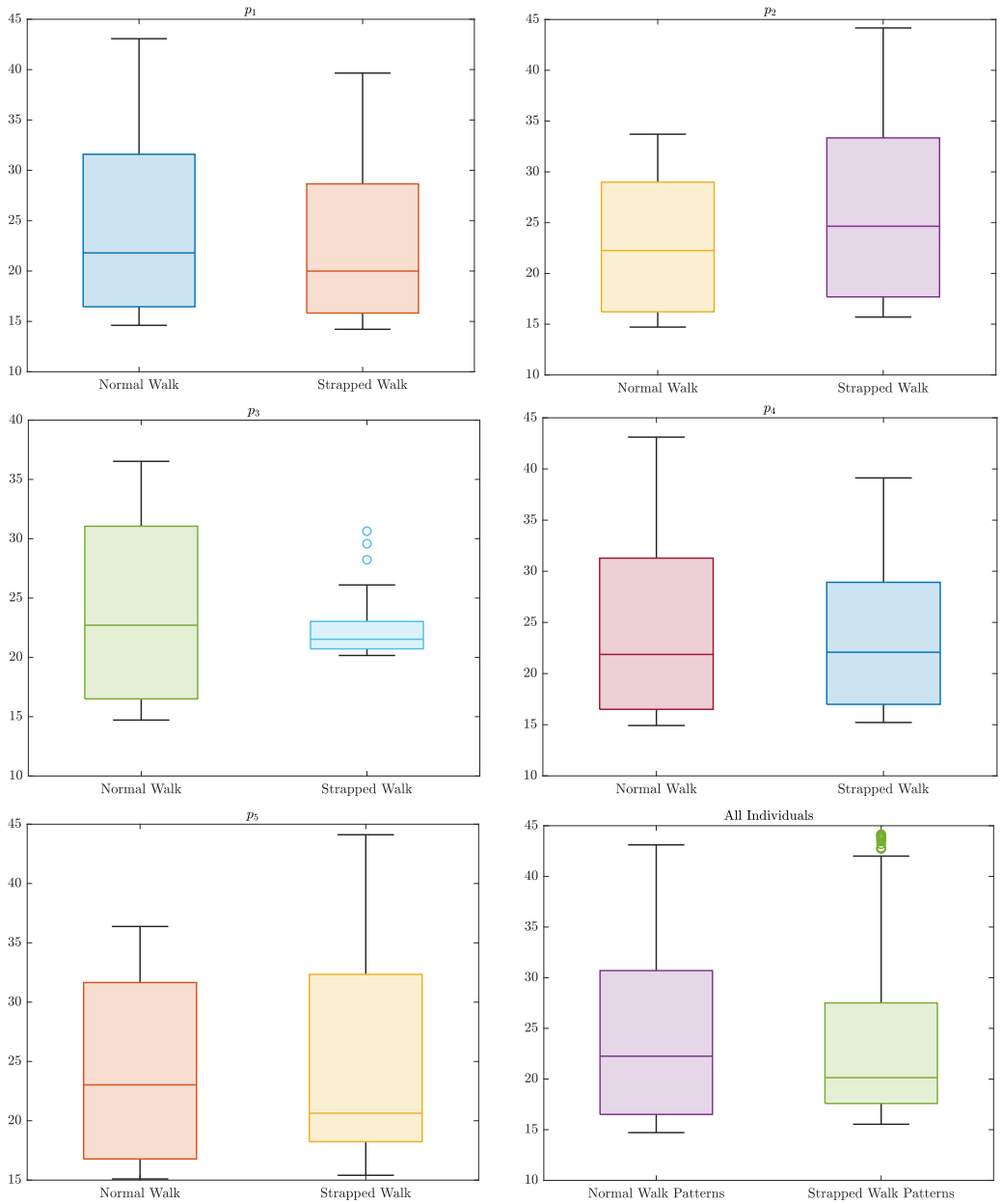

Figure 14. This figure shows the spatiotemporal plots for each walk pattern that correspond to each individual and to all individuals from the same category.

Table 3. The median of p_1, p_2, p_3, p_4 and p_5.

Category	Median				
	p_1	p_2	p_3	p_4	p_5
Normal Walk	21.804	22.252	22.709	21.869	23.029
Strapped Walk	19.99	24.645	21.527	22.085	20.637

Table 4 displays the median values of all individuals for each gait category. It shows that the median of individuals with strapped gait is lower than that of those with healthy walk patterns, and this is because of the existence of outliers in their data, as expected in the bottom right graph of Figure 14.

Table 4. The median of all individuals.

Category	Median
	All Individuals
Normal Walk	22.253
Strapped Walk	20.130

5.4.3. Histogram Analysis

Figures 15–19 visually show the histogram of individual features and their respective frequencies that describe the unique statistical characteristics of the distribution of CA data. The average mean shown in Table 5 of the strapped walk distribution is much higher than the normal walk distribution. In addition, it is obvious that the CA data distribution for the strapped walk category is somehow skewed to the right, as can be expected for individuals p_1, p_2, p_4 and p_5, whilst the distribution of p_3 is almost skewed to the left. The higher the skewness, the increased variability. The effect of the lower bound of data features on almost one side of the distribution is a major cause of the outlier occurrence, resulting from an unintentional change in experiment settings that affects the direction of distribution.

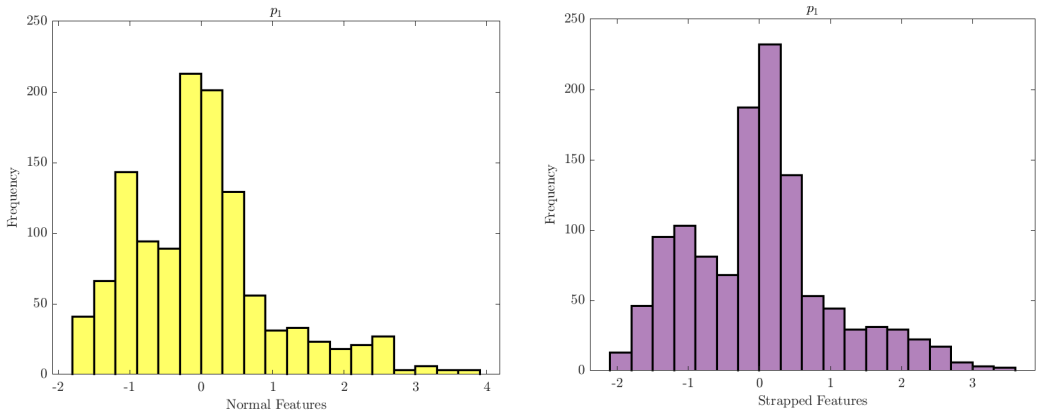

Figure 15. This figure shows the histogram plots for each walk pattern that correspond to the individual p_1.

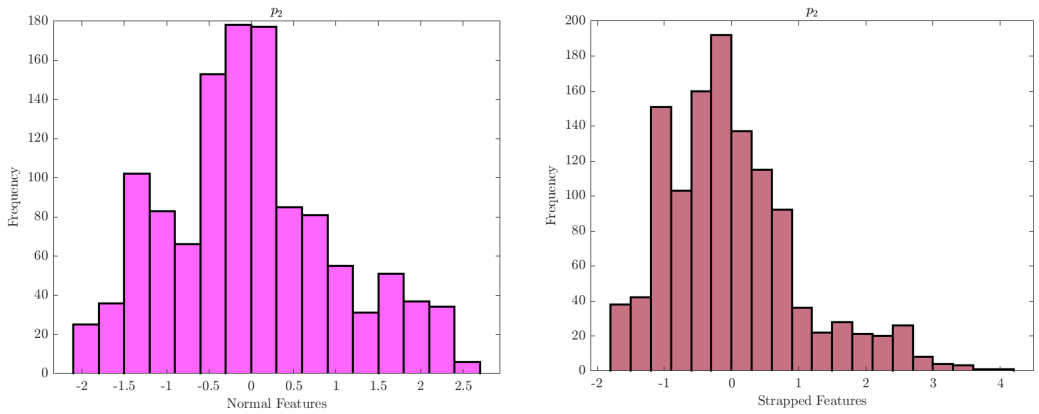

Figure 16. This figure shows the histogram plots for each walk pattern that correspond to the individual p_2.

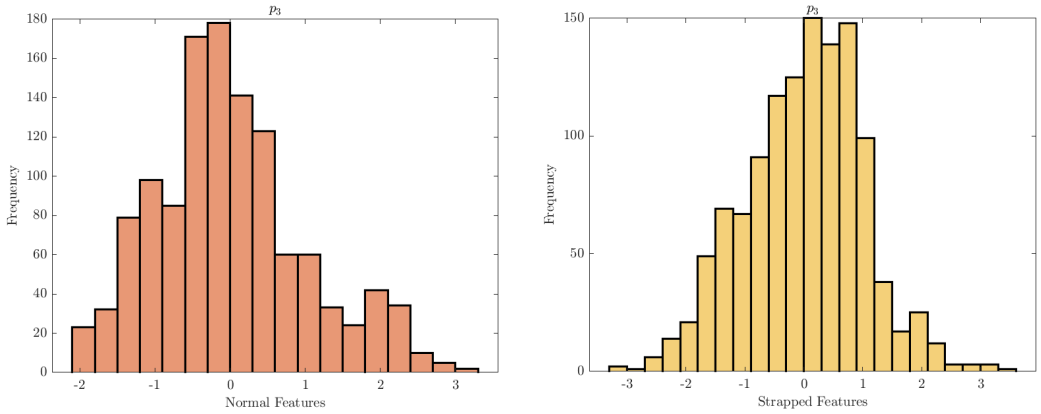

Figure 17. This figure shows the histogram plots for each walk pattern that correspond to the individual p_3.

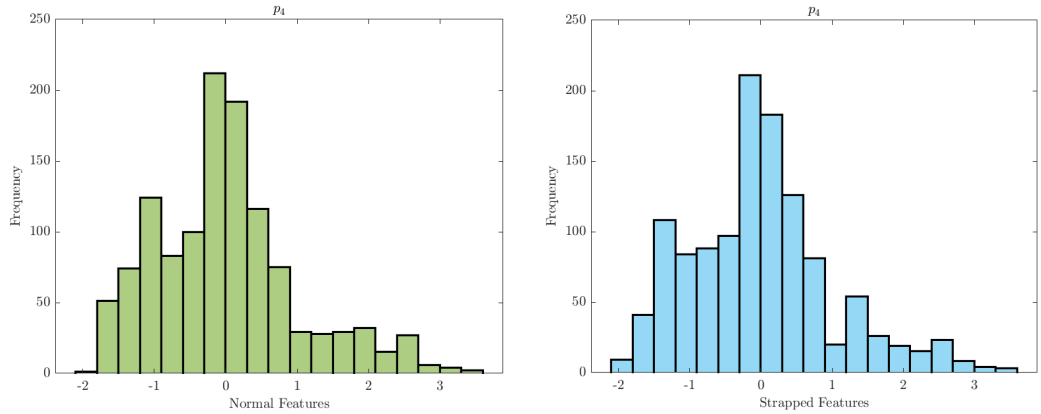

Figure 18. This figure shows the histogram plots for each walk pattern that correspond to the individual p_4.

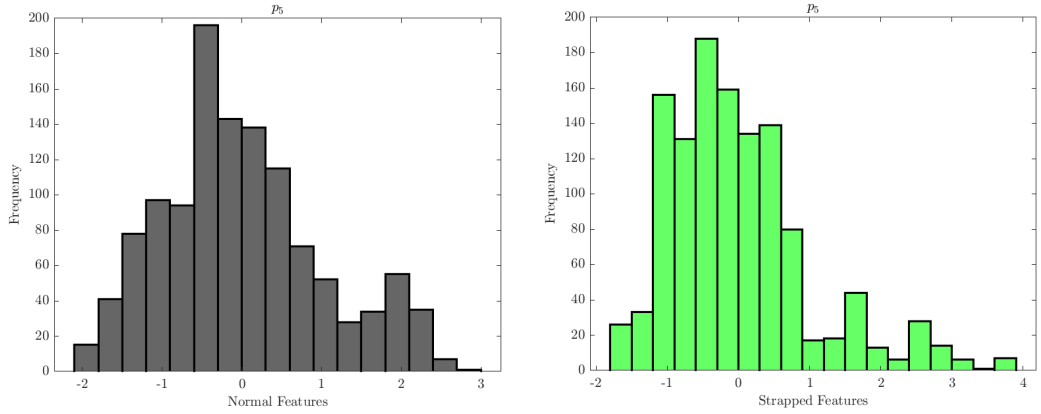

Figure 19. This figure shows the histogram plots for each walk pattern that correspond to the individual p_5.

Table 5. The mean of p_1, p_2, p_3, p_4 and p_5.

Category	**Mean**				
	p_1	p_2	p_3	p_4	p_5
Normal Walk	24.483	22.803	23.522	24.257	24.287
Strapped Walk	22.497	25.99	22.124	23.914	25.835

Figure 20 shows the distribution of data samples for each walk pattern of individuals from the same gait category, and Table 6 displays the mean values of all individuals for each gait category. It also illustrates that the mean values of individuals with strapped walk patterns are slightly lower than those with healthy walk patterns, and this is because of the existence of outliers associated with their data, as expected in the bottom right graph of Figure 20.

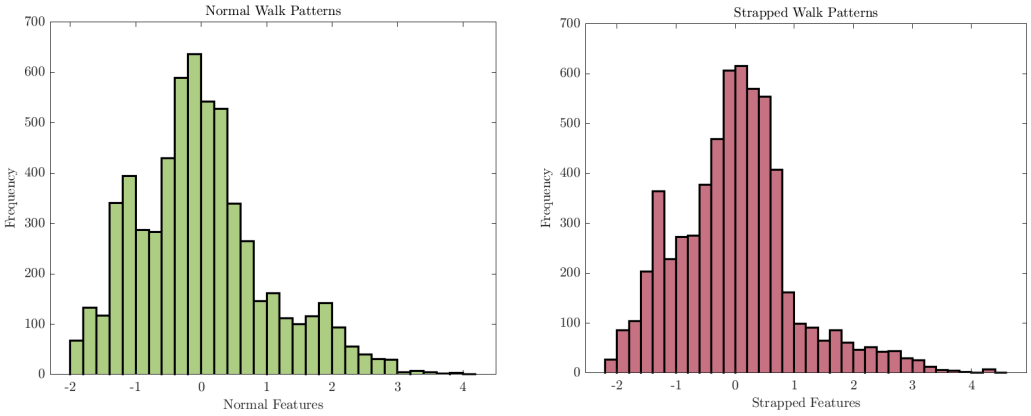

Figure 20. This figure shows the histogram plots for each walk pattern of individuals from the same gait category.

Table 6. The mean of all individuals.

Category	Mean
	All Individuals
Normal Walk	23.838
Strapped Walk	23.198

5.5. SVM Classifier

The proposed SVM model is based on the use of the kernel property discussed in Section 4.2. The most dominant extracted gait features (f of Equation (5) on the x-axis and m of Equation (4) on the y-axis) by the RCC Berry model seems to be highly correlated and nonlinear. The Kernel SVM is capable of handling and transforming the nonlinear dynamic gait data samples into a new feature space in order to facilitate the classification process of various data subjects. The extracted features by the controlled CA model were used as input to the SVM algorithm for training and for testing the classification performance of various models. The SVM classifier is trained and tested on the nonlinear CA extracted features for each individual of various gait subjects, where the two-dimensional normal and strapped walk subjects are used for training and testing, respectively. The scenario is repeated to train the Kernel SVM on all individuals data, where the normal patterns were used for training and the strapped ones were utilised for testing in order to reduce the number of parameters that could produce an unnecessary overfitting dilemma in training the gait data. The main reason for performing these two experiments is to evaluate the performance of the SVM and to examine its ability in terms of classifying various dynamic gait subjects and how it can detect the disturbances associated with individual walk behaviour. Algorithm 1 describes the implementation procedures of the proposed SVM algorithm.

5.6. SVM Model Training

There are 3000 data points in total for each gait subject (normal or strapped) and distributed equally among the five participants, so the net sum is 6000 data samples for both subjects that corresponds to both input CA extracted features. Each individual per gait category has 600 data samples. The splitting ratio used in training and testing the Kernel SVM is set to 50%. All the CA gait features were normalised using the z-score to settle

the data samples at a zero mean and unity standard deviation prior to the SVM algorithm training process. The Kernel SVM algorithm is implemented in MATLAB, including the statistical analysis of gait data and for developing various Kernel SVM models to examine the behaviour of the Kernel characteristics (regularisation parameter C and control width σ) on the classification performance of gait data. The generalisation performance of the trained Kernel SVM was evaluated by recording the prediction accuracy for each model, the confusion matrix, the Receiver Operating Characteristics (ROC) curve, and the area under the ROC curve. Details on this are discussed in the next following sections.

Algorithm 1 Pseudocode of SVM Implementation

1: **Input:** Given a training set $\Omega = (\boldsymbol{x_i}, y_i) : \boldsymbol{x_i} \in \mathbb{R}^m, y_i \in \{-1, +1\}, i = \{1, 2, \ldots, N\}$ and testing dataset $\boldsymbol{x} \in \mathbb{R}^m$.
2: **Output:** Predict subjects label for testing data $\boldsymbol{x}$.
3: Select a regularisation parameter C such that $C > 0$ and choose an appropriate kernel width control variable σ for validation.
4: Compute Gaussian Kernel RBF $\kappa(\boldsymbol{x}_i, \boldsymbol{x}_j) = \exp\left(\frac{-\|\boldsymbol{x}_i - \boldsymbol{x}_j\|^2}{2\sigma^2}\right)$.
5: Solve the kernalised optimisation problem in Equation (15) using CVX optimisation solver [18] in MATLAB.
6: Obtain optimal value of β in Equation (15) and the bias b in Equation (13).
7: Predict labels for testing data $\boldsymbol{x}$.
8: Obtain performance measure (confusion matrix, accuracy, Receiver Operating Characteristics (ROC) Curve.

5.7. Confusion Matrix

In such a binary classification problem, the dataset labels can be either positive or negative, in which the decision made by the SVM classifier can be represented by a structured contingency table known as a confusion matrix. The confusion matrix is a collection of actual and predicted binary classification information and can be used to check for the ability of the classification algorithm in distinguishing between various categories (normal or strapped). It has four main characteristics [19]:

- **True Positive** (TP): refers to the number of positive data samples (participants of normal walk) that are correctly classified and detected as positive (normal).
- **False Positive** (FP): refers to the number of negative data samples (participants of strapped walk) that are incorrectly classified as positive (normal).
- **True Negative** (TN): refers to the number of negative data samples (participants of strapped walk) that are correctly classified as negative (strapped).
- **False Negative** (FN): refers to the number of positive data samples (participants of normal walk) that are incorrectly classified as negative (strapped).

The other performance metrics of a classifier are accuracy, precision, F_1-Score, Recall or Sensitivity or True Positive Rate (TPR), Specificity or True Negative Rate (TNR), and False Positive Rate (FPR), which are evaluated on the basis of the above-stated TP, FP, TN, and FN numbers. Their definitions are as follows:

- **Accuracy**: represents the overall success rate of correct predictions. It is mathematically expressed as the ratio between the correctly classified labels $(TP + TN)$ and the total number of data samples $(TP + TN + FP + TN)$. It is given by:

$$Accuracy = \frac{TP + TN}{TP + TN + FP + TN}.$$

- **Precision**: is the ratio of correctly predicted positive labels with normal walk status to the total labels predicted to have a normal walk condition. It is measured by the following expression:

$$Precision = \frac{TP}{TP + FP}.$$

- **Recall (TPR)**: is defined as the proportion of correctly predicted positive labels with normal walk status among all normal walk data samples. It is measured by the following expression:
$$Recall = \frac{TP}{TP + FN}.$$
- **F_1-Score**: is known as the F measure, which preserves the equilibrium between the precision and the recall. It is measured as:
$$F_1\text{-}Score = \frac{2 \times Precision}{Precision + Recall}.$$
- **True Negative Rate (TNR)**: is defined as the proportion of correctly predicted negative labels with strapped walk conditions among all strapped walk data samples. It is formulated as:
$$TNR = \frac{TN}{TN + FP}.$$
- **False Positive Rate (FPR)**: is measured as the proportion of the strapped walk samples mislabeled as normal walk data among all the strapped data samples. It is given as:
$$FPR = \frac{FP}{FP + TN}.$$

The purpose of the above outlined metrics is to test the capability of the proposed SVM algorithm to detect the irregular gait patterns associated with different individuals. Appendix A summarises the performance metrics of the SVM classifier for each individual at certain values of regularisation parameters $C = (0.1, 1, 10)$, respectively. Therefore, the main validation metric measure that gives insight into the details of the overall performance of the SVM classifier is the accuracy. The accuracy of the classifier depends on the value of σ and C. Overall, the best performance was achieved when $\sigma = 0.1$ and 1.

6. Results

To better evaluate the effectiveness of the proposed methodology outlined above, the following performance measures are followed:

6.1. Receiver Operating Characteristic (ROC) Curve

The ROC plot provides an extra step towards evaluating the performance of the SVM classifier. The ROC curve visualises representative plots of TPR or sensitivity versus the ($\approx 1 - TNR$) over a range of threshold levels that varies between 0 and 1. In Figures 21–26, the ROC curves were plotted for the best pair of σ and C values that satisfy the highest accuracy during the overall trial period for each individual and for all individuals (as shown in Figure 26). It is shown that the Kernel SVM performed well in most of the cases between detecting normal and strapped features per individual and also between the different gait subjects of all individuals accordingly. Figure 27, which supports the results obtained in the left graph of Figure 26, for instance, shows the decision boundary when the SVM is trained on all individuals' walk normal patterns versus those of that strapped one, and this proves the robustness of the Kernel SVM as a universal model in detecting gait dynamics or abnormalities apart away from normal patterns. The best performance of the SVM model is well observed when $\sigma = 0.1$ and 1 for various values of C.

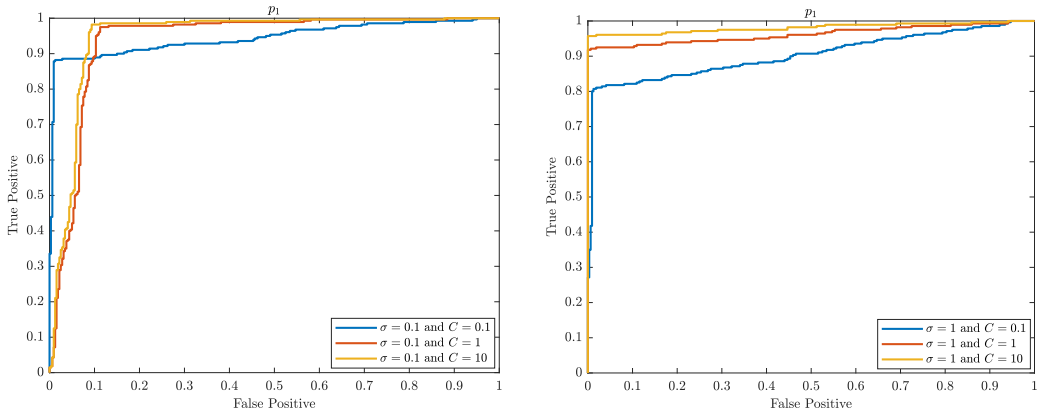

Figure 21. ROC (Receiver Operating Characteristic) curves of p_1 show the True Positive (Sensitivity) and False Positive (1-Specificity) for the best different thresholds using kernel property of SVM.

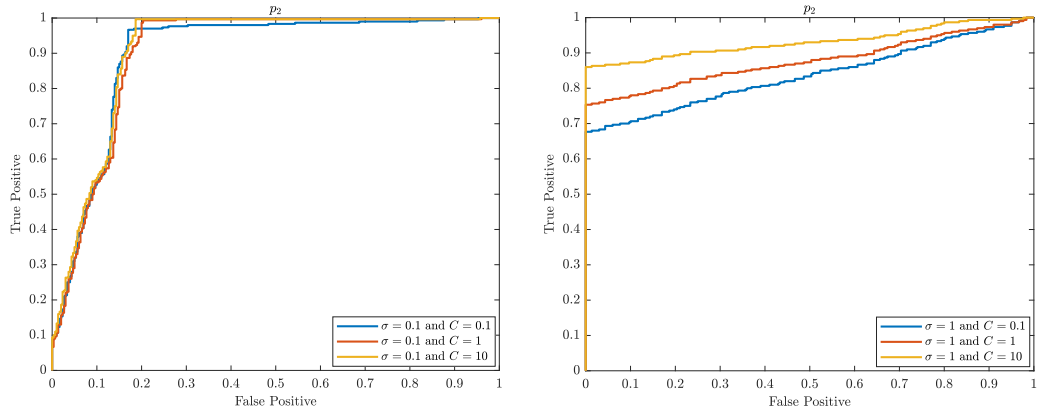

Figure 22. ROC (Receiver Operating Characteristic) curves of p_2 show the True Positive (Sensitivity) and False Positive (1-Specificity) for the best different thresholds using kernel property of SVM.

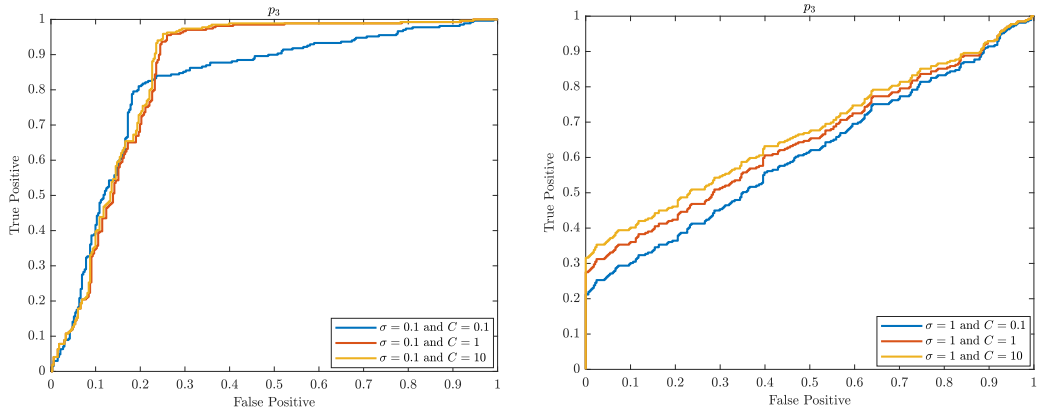

Figure 23. ROC (Receiver Operating Characteristic) curves of p_3 show the True Positive (Sensitivity) and False Positive (1-Specificity) for the best different thresholds using kernel property of SVM.

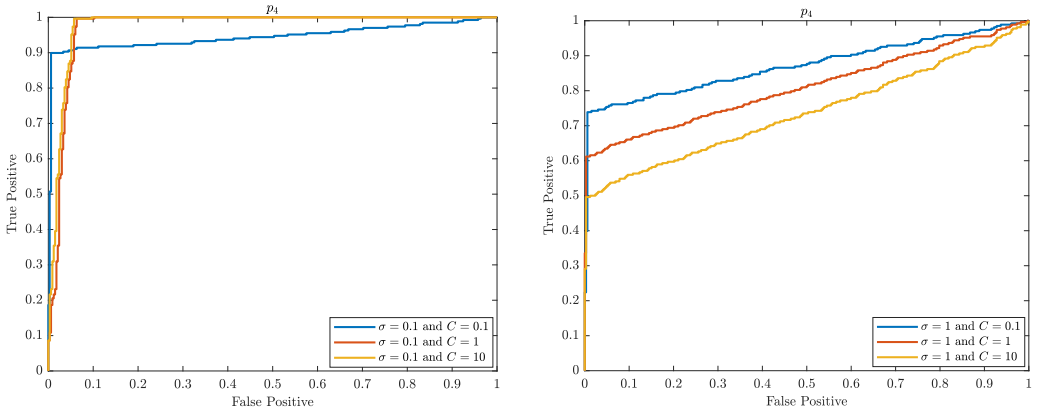

Figure 24. ROC (Receiver Operating Characteristic) curves of p_4 show the True Positive (Sensitivity) and False Positive (1-Specificity) for the best different thresholds using kernel property of SVM.

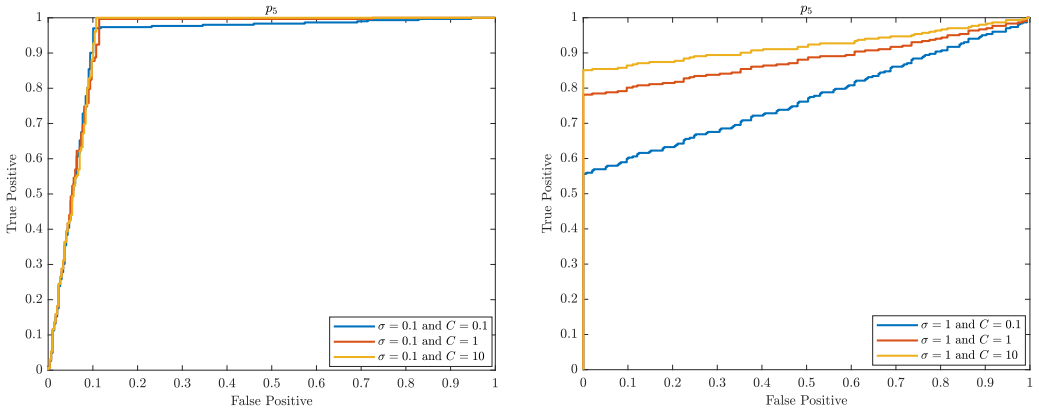

Figure 25. ROC (Receiver Operating Characteristic) curves of p_5 show the True Positive (Sensitivity) and False Positive (1-Specificity) for the best different thresholds using kernel property of SVM.

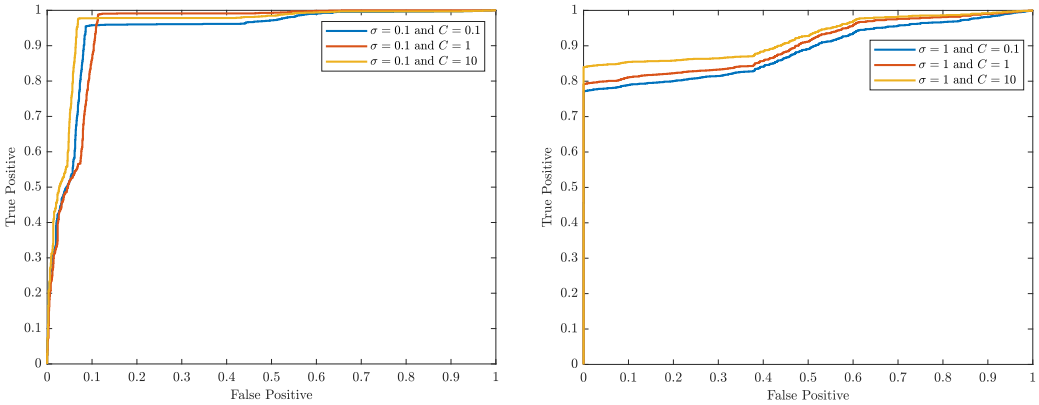

Figure 26. ROC (Receiver Operating Characteristic) curves of all individuals' gait subjects show the True Positive (Sensitivity) and False Positive (1-Specificity) for the best different thresholds using kernel property of SVM.

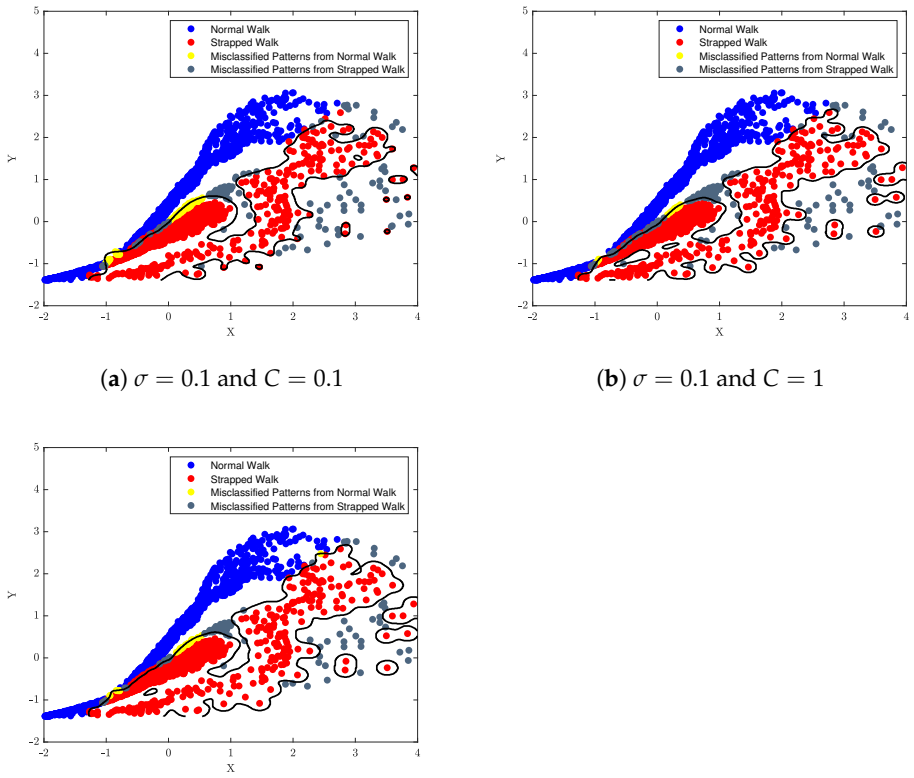

(**a**) $\sigma = 0.1$ and $C = 0.1$ (**b**) $\sigma = 0.1$ and $C = 1$

(**c**) $\sigma = 0.1$ and $C = 10$

Figure 27. The decision boundary when the SVM model trained on all individuals' normal walk patterns versus that of the strapped one, when: (**a**) $\sigma = 0.1$ and $C = 0.1$, (**b**) $\sigma = 0.1$ and $C = 1$, and (**c**) $\sigma = 0.1$ and $C = 10$.

6.2. The Area Under the Curve (AUC)

The Area Under the Curve (AUC) estimation or ROC area is chosen to represent the degree of separability by the SVM classifier. Similarly, the higher the AUC, the better the classifier is at detecting gait abnormalities of individuals. The ROC area of the Gaussian kernel as a function of the regularisation parameter C for each individual walk is illustrated in Figure 28. Knowingly, the C parameter can affect the performance of the SVM classifier, and there is a certain value or range that can maintain a better efficiency among others.

It is concluded from the performance measure shown in Tables A1–A6 of Appendix A that the SVM classifier achieves the best results when $\sigma = 0.1$ and in some cases when $\sigma = 1$, in comparison to other σ values. Based on that, the visualisation of Figure 28 is produced, and as shown, for example, there is a range of C values that would produce an optimum performance. It is also shown from Figure 28 that for some individuals, the higher the sensitivity level, the larger the Area under the Curve and the better the performance is. It is also evident from the SVM model measurements displayed in Appendix A that the values of AUC and the accuracy are much closer to each other, which means that the proposed SVM algorithm is highly efficient in classifying between normal and strapped gait disturbances. The AUC was performed computationally using our algorithm software routines developed in MATLAB. Figure 29 shows the average mean square error (MSE) rate of the SVM model for the five individuals' data. The average MSE for each individual was computed using the average accuracy for each curve shown in Figure 28. The average MSE of p_1 and p_4 was less than <6% with minimum variation rates, respectively, in classifying the gait abnormalities patterns, whereas when compared with p_2, p_3 and p_5 individuals, the average MSE and the average standard deviation proved to be extremely high.

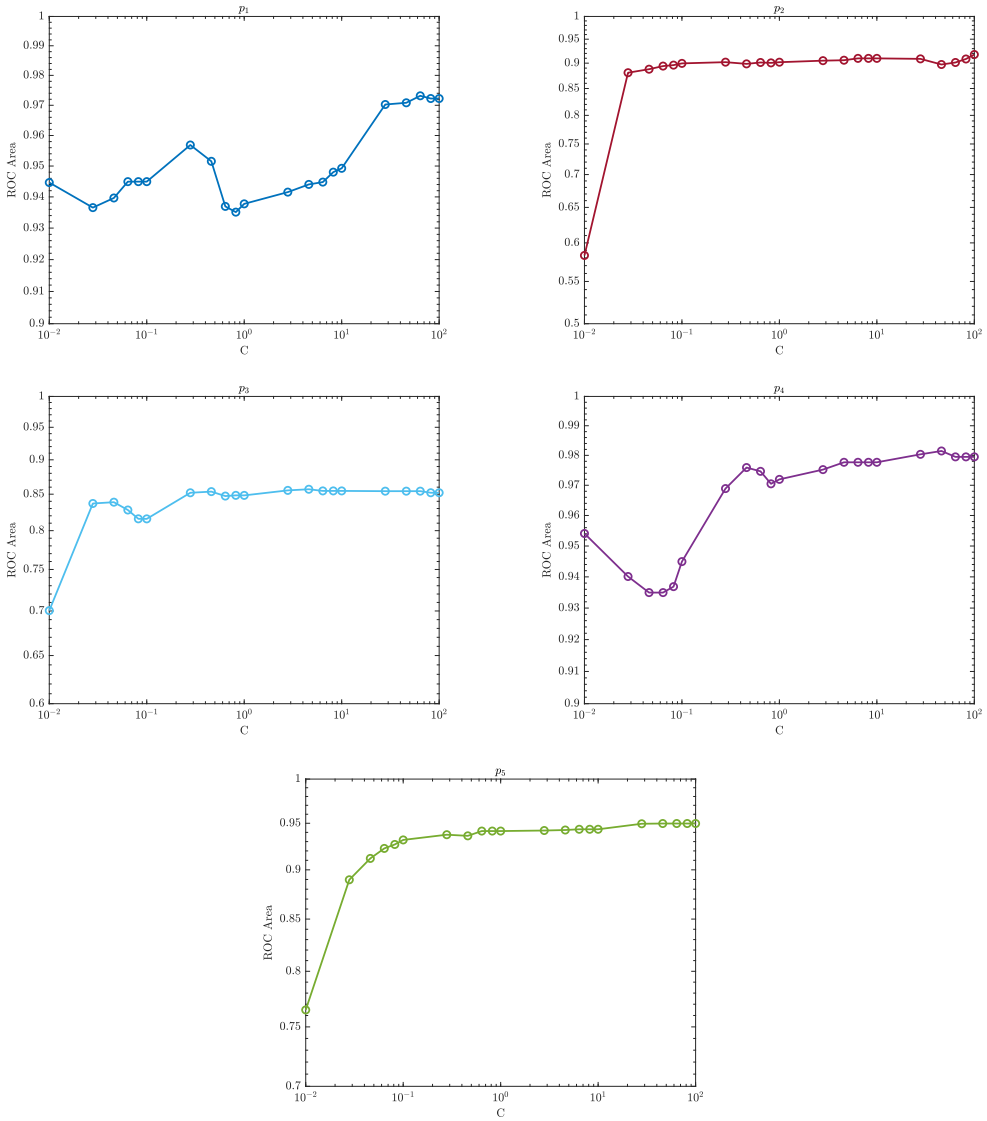

Figure 28. The ROC area or Area under ROC curve (AROC) versus various values of the regularisation parameter C when $\sigma = 0.1$ for each individual p_1, p_2, p_3, p_4, and p_5, respectively.

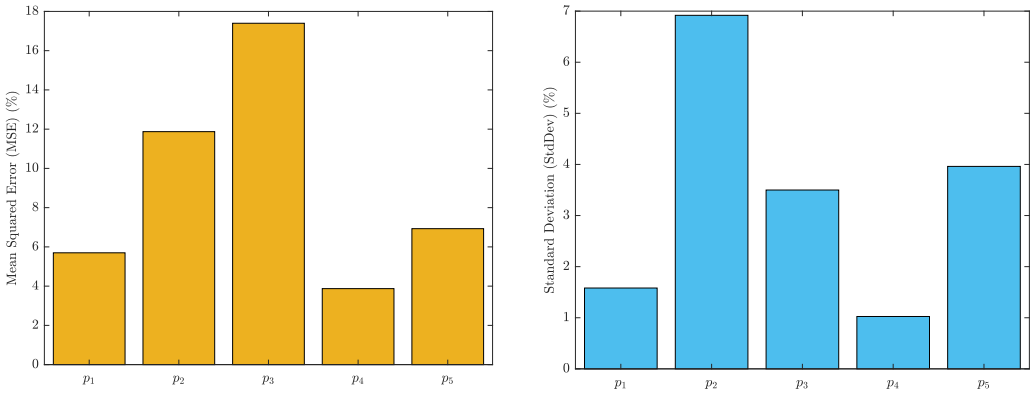

Figure 29. This figure shows the average mean square error (MSE) (%) (**on the left**) and the average standard deviation (%) (**on the right**) of the SVM classification performance for each individual piece of data.

7. Discussion

In this paper, a Support Vector Machine based on the novel proposed criticality analysis technique is implemented to classify and to detect the dynamic abnormalities and disturbance patterns associated with human gait. The results of this research paper suggest that the gait features extracted from and represented by the criticality analysis methodology provide valuable information regarding the characteristics of dynamics of human walking behaviour such that these generated patterns can be used to train such a machine learning model to automate and recognise the walking deviations from the normal walk of individuals. Early detection of human gait disturbances using such a supervised pattern recognition technique would enhance the chance to identify gait impairments and to prevent gait injuries as well. Neural Networks (NNs) and fuzzy clustering techniques have been used in previous research work on automated gait classification for diagnosing pathological human gait [20–22]. Due to the superior gait classification performance as shown in this paper, the SVM with the support of the CA method can perform as a robust and reliable classification tool for the detection of dynamic disturbances of biological data patterns and creates a tremendous opportunity for clinical diagnosis and rehabilitation.

In this research, the extracted data from the CA method have been used as inputs to the SVM to represent various gait patterns. The reason for this is twofold; firstly, the CA-extracted data provide a more realistic measure of the kinematic motor system and describe a deep representation of the dynamics disturbing the individual gait, and secondly, the kernalised nonlinear property of the SVM makes the classification process of the CA data patterns, which are in fact nonlinear, more detectable and identifiable. Furthermore, the CA methodology creates sufficient data samples so that their properties can lead to a real analysis of human gait. An insufficient or limited number of gait samples due to data measurements over a short period of time can deteriorate the distribution of data and thus result in poor classification performance. To derive more controlled and stable CA data patterns of human gait, the pre-processed raw data are recorded for a long walk cycle period of 6 s to provide a reliable and useful statistical distribution of gait patterns.

The classification performance of the proposed Kernel SVM primarily relies on the best selection of the regularisation parameter C, as depicted in Figure 28 and also in Tables A1–A6 of Appendix A. C is used as a penalty parameter to compensate for the misclassification accuracy, and it has to be engineered carefully in order to achieve maximum performance accuracy. When the classification performance was compared to three different regularisation parameters C that mapped to three control width values of σ, the performance of SVM is found to perform well when $\sigma = 0.1$, which is followed by $\sigma = 1$. This is because the smaller the value of σ, the quicker is the rate of decline of the Kernel Gaussian function. The use of the Kernel Gaussian function in the implementation of the SVM was found to perform the best in detecting the abnormal disturbances of gait data patterns. This was obvious from their recorded accuracy at these specific values. In addition, Figure 28 shows that the optimal value of C changes according to individual data patterns. The parameter C can be selected based on the trial and error method, and one way to achieve this is to visualise the dependency of the classification performance on C. The classification results of this research suggest that the proposed SVM models with the support of the CA method can perform as a robust and reliable classification tool for the detection of dynamic disturbances of human gait data patterns. The generalisation performance of such a classification tool mainly depends on targeting the best features that have great potential to result in a good performance. Interestingly, the CA method is proposed in this research paper to not only select a few data features but to represent the whole data samples of features without exclusion to some others. The results illustrated in Figures 2–7 show that the gait disturbances and changes to the normal walk patterns can be detectable and distinguishable by observation, and even without machine learning training. Many research studies have been conducted on feature selection tools for better choosing the most significant patterns that lead to an adequate performance such as the mean absolute deviation extended serial fusion (MDeSF) approach [23] and sequential

backward selection (SBS) approach [24], but none of these research studies ever consider the representation of multivariate data patterns for more insightful performance. To the best of our knowledge, this research paper is the only one which considered a novel criticality analysis technique for multivariate data representation that opens the horizon to applied machine learning theory.

The scatter and histogram plots of CA gait features extracted from the dynamic gait were also instrumental and informative in differentiating between the normal and strapped walk. This suggests that the dynamic gait changes with the condition or behaviour of the individual gait are reflected from their visual patterns. The histogram plots shown in Figures 15–20 provide statistical interpretation of the CA data distribution, whereas the scatter plots illustrated in Figures 8–13 discuss the variability of the CA gait data in space. In addition, these plots are useful in detecting the gait abnormalities and for observing the individual walk progression as a result of treatment in clinical settings. The CA gait features represented by the distribution and variability measures were the basis of the classification process between the two distinct gait patterns.

The research introduced in this paper can be extended further in many ways. The adoption of Graph Convolution Neural Networks (GCNNs) as a graph-based deep learning method can be viewed as a powerful structure that operates over graphs to model and to perform classification tasks to any various types of data, whether it is structured or unstructured, such as human gait dynamic data. With the help of Graph Kernel (GK) that can be used on pairs of graphs to map the similarity between two graphs of data subjects by comparing their substructures or subgraphs, the GK can convert the human gait cycle into graph signals with convenient graph structures and signal features used as input to the GCNNs to detect the gait dynamics observable by humans and to enhance the classification accuracy. This idea will be explored further in future research.

8. Conclusions

The implemented SVM model based on the proposed CA technique serves as a dominant tool for classifying human gait patterns and detecting disturbances that affect healthy walk in humans. The CA methodology is characterised by its ability to extract and to represent the most useful gait features in a reduced two-dimensional space. The improved performances of the SVM models were evident when data were trained with the CA method and with the kernelised properties of the SVM models. The simulated results of this research showed that the proposed SVM model with the support of the CA method can perform as a robust and reliable classification candidate for the detection of dynamic disturbances of biological data patterns and creates a tremendous opportunity for clinical diagnosis and rehabilitation.

Author Contributions: Conceptualisation, S.E.; methodology, S.E.; validation, S.E.; formal analysis, S.E.; investigation, S.E.; data curation, H.D.; writing—original draft preparation, S.E.; writing—review and editing, S.E. and T.V.o.S.; visualisation, S.E.; supervision, T.V.o.S. All authors have read and agreed to the published version of the manuscript.

Funding: This research received no external funding.

Institutional Review Board Statement: Not applicable.

Informed Consent Statement: Not applicable.

Data Availability Statement: Due to the General Data Protection Regulation (GDPR) guidelines, the database used in this paper is kept private and secure under the cohort of the Faculty of Health Sciences at Oxford Brookes University.

Acknowledgments: The authors gratefully acknowledge the Faculty of Health Sciences at Oxford Brookes University for their technical support and for being the main data provider to carry out this research work.

Conflicts of Interest: The authors declare no conflict of interest.

Appendix A

Table A1. SVM Classification Results of p_1 Walk Patterns.

Performance	$\sigma = 0.1$		
	$C = 0.1$	$C = 1$	$C = 10$
TP	317	283	289
FP	34	7	5
FN	3	37	31
TN	246	273	275
FPR	0.121	0.025	0.017
Precision	0.903	0.975	0.982
Recall	0.990	0.884	0.903
F1-Score	0.944	0.927	0.941
Specificity	0.878	0.975	0.982
AROC	0.944	0.937	0.949
Accuracy(%)	93.83	92.67	94
Performance	$\sigma = 1$		
	$C = 0.1$	$C = 1$	$C = 10$
TP	316	320	320
FP	54	23	12
FN	4	0	0
TN	226	257	268
FPR	0.192	0.082	0.042
Precision	0.854	0.932	0.963
Recall	0.987	1	1
F1-Score	0.915	0.965	0.981
Specificity	0.807	0.917	0.957
AROC	0.902	0.962	0.981
Accuracy(%)	90.33	96.17	98
Performance	$\sigma = 10$		
	$C = 0.1$	$C = 1$	$C = 10$
TP	320	320	320
FP	280	280	280
FN	0	0	0
TN	0	0	0
FPR	1	1	1
Precision	0.533	0.533	0.533
Recall	1	1	1
F1-Score	0.695	0.695	0.695
Specificity	0	0	0
AROC	0.519	0.519	0.519
Accuracy(%)	53.33	53.33	53.33

Table A2. SVM Classification Results of p_2 Walk Patterns.

Performance	$\sigma = 0.1$		
	$C = 0.1$	$C = 1$	$C = 10$
TP	249	239	244
FP	10	2	1
FN	51	61	56
TN	290	298	299
FPR	0.033	0.006	0.003
Precision	0.961	0.991	0.995
Recall	0.83	0.796	0.813
F1-Score	0.89	0.883	0.895
Specificity	0.966	0.993	0.996
AROC	0.899	0.901	0.909
Accuracy(%)	98.83	89.5	90.5

Table A2. *Cont.*

Performance	$\sigma = 1$		
	$C = 0.1$	$C = 1$	$C = 10$
TP	300	300	300
FP	97	74	42
FN	0	0	0
TN	203	226	258
FPR	0.323	0.246	0.14
Precision	0.755	0.802	0.877
Recall	1	1	1
F1-Score	0.86	0.89	0.934
Specificity	0.676	0.753	0.86
AROC	0.837	0.877	0.931
Accuracy(%)	83.83	87.67	93
Performance	$\sigma = 10$		
	$C = 0.1$	$C = 1$	$C = 10$
TP	300	300	300
FP	300	300	300
FN	0	0	0
TN	0	0	0
FPR	1	1	1
Precision	0.5	0.5	0.5
Recall	1	1	1
F1-Score	0.667	0.667	0.667
Specificity	0	0	0
AROC	0.504	0.504	0.504
Accuracy(%)	50	50	50

Table A3. SVM Classification Results of p_3 Walk Patterns.

Performance	$\sigma = 0.1$		
	$C = 0.1$	$C = 1$	$C = 10$
TP	265	244	247
FP	51	12	11
FN	66	87	84
TN	218	257	258
FPR	0.189	0.044	0.04
Precision	0.838	0.953	0.957
Recall	0.8	0.737	0.746
F1-Score	0.81	0.955	0.959
Specificity	0.81	0.955	0.959
AROC	0.815	0.848	0.854
Accuracy(%)	80.5	83.5	84.17
Performance	$\sigma = 1$		
	$C = 0.1$	$C = 1$	$C = 10$
TP	331	331	331
FP	212	195	184
FN	0	0	0
TN	57	74	85
FPR	0.788	0.724	0.684
Precision	0.609	0.629	0.642
Recall	1	1	1
F1-Score	0.757	0.772	0.782
Specificity	0.211	0.275	0.315
AROC	0.611	0.648	0.673
Accuracy(%)	64.67	67.5	69.33

Table A3. *Cont.*

Performance	$\sigma = 10$		
	$C = 0.1$	$C = 1$	$C = 10$
TP	331	331	331
FP	269	269	269
FN	0	0	0
TN	0	0	0
FPR	1	1	1
Precision	0.551	0.551	0.551
Recall	1	1	1
F1-Score	0.711	0.711	0.711
Specificity	0	0	0
AROC	0.504	0.504	0.504
Accuracy(%)	55.17	55.17	55.17

Table A4. SVM Classification Results of p_4 Walk Patterns.

Performance	$\sigma = 0.1$		
	$C = 0.1$	$C = 1$	$C = 10$
TP	330	311	313
FP	27	1	1
FN	2	21	19
TN	241	267	267
FPR	0.1	0.003	0.003
Precision	0.924	0.996	0.996
Recall	0.993	0.936	0.942
F1-Score	0.957	0.965	0.969
Specificity	0.899	0.996	0.996
AROC	0.944	0.971	0.977
Accuracy(%)	95.17	96.33	96.67
Performance	$\sigma = 1$		
	$C = 0.1$	$C = 1$	$C = 10$
TP	330	331	331
FP	70	104	135
FN	2	1	1
TN	198	164	133
FPR	0.261	0.388	0.503
Precision	0.825	0.76	0.71
Recall	0.993	0.996	0.996
F1-Score	0.901	0.863	0.829
Specificity	0.738	0.611	0.496
AROC	0.871	0.81	0.738
Accuracy(%)	88	82.5	77.33
Performance	$\sigma = 10$		
	$C = 0.1$	$C = 1$	$C = 10$
TP	332	332	332
FP	268	268	268
FN	0	0	0
TN	0	0	0
FPR	1	1	1
Precision	0.553	0.553	0.553
Recall	1	1	1
F1-Score	0.712	0.712	0.712
Specificity	0	0	0
AROC	0.502	0.502	0.502
Accuracy(%)	55.33	55.33	55.33

Table A5. SVM Classification Results of p_5 Walk Patterns.

Performance	$\sigma = 0.1$		
	$C = 0.1$	$C = 1$	$C = 10$
TP	268	264	266
FP	9	1	0
FN	30	34	32
TN	293	301	302
FPR	0.029	0.003	0
Precision	0.967	0.996	1
Recall	0.899	0.885	0.892
F1-Score	0.932	0.937	0.943
Specificity	0.97	0.996	1
AROC	0.931	0.941	0.943
Accuracy(%)	93.5	94.17	94.67
Performance	$\sigma = 1$		
	$C = 0.1$	$C = 1$	$C = 10$
TP	298	298	298
FP	134	66	45
FN	0	0	0
TN	168	236	257
FPR	0.443	0.218	0.149
Precision	0.689	0.818	0.868
Recall	1	1	1
F1-Score	0.816	0.9	0.929
Specificity	0.556	0.781	0.85
AROC	0.769	0.88	0.92
Accuracy(%)	77.67	89	92.5
Performance	$\sigma = 10$		
	$C = 0.1$	$C = 1$	$C = 10$
TP	298	298	298
FP	302	302	302
FN	0	0	0
TN	0	0	0
FPR	1	1	1
Precision	0.496	0.496	0.496
Recall	1	1	1
F1-Score	0.663	0.663	0.663
Specificity	0	0	0
AROC	0.495	0.495	0.495
Accuracy(%)	49.67	49.67	49.67

Table A6. SVM Classification Results of All Individuals Walk Patterns.

Performance	$\sigma = 0.1$		
	$C = 0.1$	$C = 1$	$C = 10$
TP	1480	1435	1507
FP	62	16	32
FN	139	184	112
TN	1319	1365	1349
FPR	0.044	0.011	0.023
Precision	0.959	0.988	0.979
Recall	0.914	0.886	0.930
F1-Score	0.936	0.934	0.954
Specificity	0.955	0.988	0.976
AROC	0.939	0.945	0.957
Accuracy(%)	93.3	93.33	95.2

Table A6. *Cont.*

Performance	$\sigma = 1$		
	$C = 0.1$	$C = 1$	$C = 10$
TP	1618	1619	1619
FP	316	288	221
FN	1	0	0
TN	1065	1093	1160
FPR	0.228	0.208	0.16
Precision	0.836	0.848	0.879
Recall	0.999	1	1
F1-Score	0.91	0.918	0.936
Specificity	0.771	0.791	0.839
AROC	0.886	0.903	0.924
Accuracy(%)	89.43	90.4	92.63
Performance	$\sigma = 10$		
	$C = 0.1$	$C = 1$	$C = 10$
TP	1619	1619	1619
FP	1381	1381	1381
FN	0	0	0
TN	0	0	0
FPR	1	1	1
Precision	0.539	0.539	0.539
Recall	1	1	1
F1-Score	0.701	0.701	0.701
Specificity	0	0	0
AROC	0.50	0.50	0.50
Accuracy(%)	53.96	53.96	53.96

References

1. Eltanani, S.; Scheper, T.O.; Dawes, H.K. Nearest Neighbor Algorithm: Proposed Solution for Human Gait Data Classification. In Proceedings of the IEEE Symposium on Computers and Communications (ISCC), Athens, Greece, 5–8 September 2021. [CrossRef]
2. olde Scheper, T.V. Biologically Inspired Rate Control of Chaos. Chaos: An Interdiscip. *J. Nonlinear Sci.* **2017**, *27*, 103122. [CrossRef]
3. Berry, H. Chaos in a Bienzymatic Cyclic Model with Two Autocatalytic Loops. *Chaos Solitons Fractals* **2003**, *18*, 1001–1014. [CrossRef]
4. olde Scheper, T.V. Self-Organised Criticality Equation Files [Data set]. *Zenodo* **2021**. [CrossRef]
5. olde Scheper, T.V. Criticality in Biocomputation. In Proceedings of the European Symposium on Artificial Neural Networks, Computational Intelligence and Machine Learning, Bruges, Belgium, 26–28 April 2017; pp. 1–6.
6. Kyrychko, Y.N.; Blyuss, K.B.; Hogan, S.J.; Schöll, E. Control of Spatiotemporal Patterns in the Gray–Scott Model. *Chaos Interdiscip. J. Nonlinear Sci.* **2009**, *19*, 043126. [CrossRef] [PubMed]
7. Vapnik, V. *Statistical Learning Theory*; Wiley: New York, NY, USA, 1998.
8. Cristianini, N.; Shawe-Taylor, J. *An Introduction to Support Vector Machines and Other Kernel-Based Learning Methods*; Cambridge University Press: Cambridge, UK, 2000.
9. Hastie, T.; Tibshirani, R.; Friedman, J. *The Elements of Statistical Learning*; Springer: New York, NY, USA, 2001.
10. Boyd, S.; Vandenberghe, L. *Convex Optimization*; Cambridge University Press: Cambridge, UK, 2004.
11. Shalev-Shwartz, S.; Ben-David, S. *Understanding Machine Learning—From Theory to Algorithms*; Cambridge University Press: Cambridge, UK, 2014; pp. 1–397.
12. Que, Q.; Belkin, M. Back to the Future: Radial Basis Function Network Revisited. In *IEEE Transactions on Pattern Analysis and Machine Intelligence*; IEEE: Piscataway, NJ, USA, 2020; Volume 42, pp. 1856–1867. [CrossRef]
13. Panchapakesan, C.; Ralph, D.; Palaniswami, M. Effects of Moving the Centers in an RBF Network. In Proceedings of the IEEE International Joint Conference on Neural Networks Proceedings, IEEE World Congress on Computational Intelligence (Cat. No.98CH36227), Anchorage, AK, USA, 4–9 May 1998. [CrossRef]
14. Esser, P.; Dawes, H.; Collett, J.; Howells, K. IMU: Inertial Sensing of Vertical CoM Movement. *J. Biomech.* **2009**, *42*, 1578–1581. [CrossRef] [PubMed]
15. Esser, P.; Dawes, H.; Collett, J.; Howells, K. Insights into Gait Disorders: Walking Variability Using Phase Plot Analysis, Parkinson's Disease. *Gait Posture* **2013**, *38*, 648–652. [CrossRef]
16. AX3 GUI · digitalinteraction/openmovement Wiki. Available online: https://github.com/digitalinteraction/openmovement/wiki/AX3-GUI (accessed on 1 April 2022).
17. olde Scheper, T.V. Controlled Bio-Inspired Self-Organised Criticality. *Plos ONE* **2022**, *17*, e0260016. [CrossRef] [PubMed]

18. CVX: Matlab Software for Disciplined Convex Programming | CVX Research, Inc. 2012. Available online: http://cvxr.com/cvx (accessed on 15 May 2022).
19. Sun, L. Multi-Class Associative Classification Based on Intersection Method and Extended Chi-Square Testing. *J. Comput. Appl.* **2008**, *28*, 1692–1695. [CrossRef]
20. Varrecchia, T.; Castiglia, S.F.; Ranavolo, A.; Conte, C.; Tatarelli, A.; Coppola, G.; Di Lorenzo, C.; Draicchio, F.; Pierelli, F.; Serrao, M. An Artificial Neural Network Approach to Detect Presence and Severity of Parkinson's Disease via Gait Parameters. *PLoS ONE* **2021**, *16*, e0244396. [CrossRef] [PubMed]
21. Wang, F.-C.; Chen, S.-F.; Lin, C.-H.; Shih, C.-J.; Lin, A.-C.; Yuan, W.; Li, Y.-C.; Kuo, T.-Y. Detection and Classification of Stroke Gaits by Deep Neural Networks Employing Inertial Measurement Units. *Sensors* **2021**, *21*, 1864. [CrossRef] [PubMed]
22. Darbandi, H.; Baniasad, M.; Baghdadi, S.; Khandan, A.; Vafaee, A.; Farahmand, F. Automatic Classification of Gait Patterns in Children with Cerebral Palsy Using Fuzzy Clustering *Method. Clin. Biomech.* **2020**, *73*, 189–194. [CrossRef] [PubMed]
23. Saleem, F.; Khan, M.A.; Alhaisoni, M.; Tariq, U.; Armghan, A.; Alenezi, F.; Choi, J.-I.; Kadry, S. Human Gait Recognition: A Single Stream Optimal Deep Learning Features Fusion. *Sensors* **2021**, *21*, 7584. [CrossRef] [PubMed]
24. Trabassi, D.; Serrao, M.; Varrecchia, T.; Ranavolo, A.; Coppola, G.; De Icco, R.; Tassorelli, C.; Castiglia, S.F. Machine Learning Approach to Support the Detection of Parkinson's Disease in IMU-Based Gait Analysis. *Sensors* **2022**, *22*, 3700. [CrossRef] [PubMed]